Received: 2 October 2024 | Accepted: 16 January 2025
DOI: 10.1002/agg2.70051

Agrosystems, Geosciences & Environment OPEN ACCESS

ORIGINAL ARTICLE

Special Section: Enhancing Food Security through Innovative Agricultural Management

Nitrogen-based proximal sensing and data fusion for management zone delineation

Md Tawhid Hossain[1] | **Marco Donat**[1] | **Ines Astrid Tougma**[1] | **Sonoko D. Bellingrath-Kimura**[1,2] | **Kathrin Grahmann**[1]

[1]Leibniz Centre for Agricultural Landscape Research (ZALF), Müncheberg, Germany

[2]Institute of Agriculture and Horticulture, Faculty of Life Science, Humboldt University of Berlin, Berlin, Germany

Correspondence
Md Tawhid Hossain, Research Area 2 "Land Use and Governance," Working group: Resource-Efficient Cropping Systems, Leibniz Centre for Agricultural Landscape Research (ZALF), 15374, Müncheberg, Brandenburg, Germany.
Email: mdtawhid.hossain@zalf.de.

Assigned to Associate Editor Ron Heiniger.

Funding information
Leibniz Centre for Agricultural Landscape Research (ZALF)

Abstract

Delineation of management zones (MZ) based on soil mineral nitrogen (SMN) dynamics can enhance site-specific management, reduce nitrate leaching, and improve nutrient efficiency. We tested proximal sensing as an alternative to standard laboratory methods to capture the spatial variability of SMN, nitrate (NO_3^-), and soil moisture (SM) and combined these data with topographic and remote sensing inputs to delineate MZ using data fusion and *k*-means clustering. Two conventionally managed fields with winter oilseed rape (*Brassica napus* L.) and winter barley (*Hordeum vulgare* L.) were chosen for Field-A and Field-B. Fresh soil samples were analyzed in the laboratory using KCl extraction, while global positioning system-labeled data from a proximal soil sensor (FarmLab) were accessed via cloud storage. FarmLab estimated NO_3^- and SMN were higher than laboratory results ($p < 0.05$), whereas SM showed no significant difference between the two methods. Bland–Altman analysis, which assesses the limit of agreement between methods to ensure consistency, revealed significant discrepancies in NO_3^- estimated by both methods, particularly in Field-B, with limits of agreement ranging from −17.40 to 29.66 mg kg^{-1}. Results of *k*-means clustering, a method for grouping data into similar categories, were evaluated using 11 feature sets, which combine data from multiple sources (laboratory and FarmLab data, satellites, and topographic data) to create a comprehensive dataset for analysis at different time points in autumn and spring. The results showed that the optimal clustering result varied depending on the field and date. Feature sets with topographic variables performed well in Field-A, while feature sets with remote sensing, topography, and FarmLab data improved MZ in Field-B. This study demonstrates how the FarmLab device can capture within-field SMN variability and examines the similarities and differences between both methods (laboratory and FarmLab).

Abbreviations: DEM, digital elevation model; GRNDVI, green–red normalized difference vegetation index; MSE, mean squared error; MZ, management zone; NDRE, normalized difference red-edge index; NDVI, normalized difference vegetation index; NIR, near-infrared; SD, standard deviation; SM, soil moisture; SMN, soil mineral nitrogen; UV, ultraviolet.

This is an open access article under the terms of the Creative Commons Attribution License, which permits use, distribution and reproduction in any medium, provided the original work is properly cited.
© 2025 The Author(s). *Agrosystems, Geosciences & Environment* published by Wiley Periodicals LLC on behalf of Crop Science Society of America and American Society of Agronomy.

Despite discrepancies between methods, FarmLab showed the potential of integrating in-season NO_3^- and SMN data with topographic and remote sensing data to delineate MZ. This approach can be scaled up to farm and landscape scale, allowing farmers to leverage proximal and remote sensing data for in-season SMN monitoring, which enables efficient nutrient management and promotes sustainable farming practices with economic and environmental benefits.

Plain Language Summary

This study explores how modern technology can improve nitrogen management in farming. We used a portable soil sensor and combined its data with satellite images and land features to identify zones within fields that require different amounts of fertilizer. After testing in rapeseed and barley fields, the sensor showed potential for tracking soil nitrogen dynamics despite some differences compared to laboratory results. We created management zones tailored to the fields' unique conditions by clustering the proximal and remote sensing data. This approach may support precise fertilization, reducing nitrogen loss while improving yields. Our findings highlight the value of combining soil, satellite, and topographic data to promote sustainable agriculture.

1 | INTRODUCTION

Capturing spatio-temporal variability of soil mineral nitrogen (SMN) is crucial for crop performance as it is the primary source of nitrogen, a key nutrient supporting plant growth, chlorophyll production, and overall crop yield (Ye et al., 2022). Even at the field scale, it is challenging to track SMN and to ensure the appropriate nitrogen (N) supply throughout crop growth stages (S. Zhang et al., 2017). In large-scale cropping systems, N surplus from fertilization causes ground and surface water pollution with NO_3^- (Sundermann et al., 2020) and leads to economic burdens of water treatment for household and industrial purposes (Cullmann et al., 2022). A key challenge for spring fertilization of winter crops is to assess the spatial distribution of SMN after autumn and winter rainfall to prevent fertilizer mismanagement (Zhao et al., 2020). To determine the field variability of SMN (sum of NO_3^- and NH_4^+), high-resolution spatio-temporal sampling is needed, which is laborious and time-consuming. Although laboratory-based results are considered the gold standard, the effort and resources required can be substantial (Guerrero et al., 2021a; Viscarra Rossel & Bouma, 2016). To address the limitations of traditional laboratory methods, new data collection approaches are necessary by leveraging advanced sensing technologies. Over the decades, different proximal sensors have been developed to estimate real-time SMN (Guerrero et al., 2021b; Y. Li et al., 2019). Sensors based on electrochemical techniques such as ion-selective electrodes (ISE) (Kim et al., 2007; Y. Li et al., 2019) or ion-selective field-effect transistors (Artigas et al., 2001; Smolka et al., 2017) are known for their suitability to measure SMN. Nevertheless, these sensor technologies present challenges for real-time measurements in the field due to the necessity of preparing a soil solution and the substantial time delay needed to attain a stable measurement curve. Challenges are also associated with harsh measurement conditions, variation in the soil-to-sensor distance, and noise (Guerrero et al., 2021a; Najdenko et al., 2024). Other recent developments include all-solid-state miniature potentiometric soil sensors (Ali et al., 2019) and ultraviolet (UV) absorbance spectroscopy (Yeshno et al., 2019), yet these technologies are still in-situ and only suitable for NO_3^- determination.

Simultaneously, in contemporary precision agriculture, a common approach to mitigate NO_3^- leaching and overfertilization is the creation of management zones (MZ) by applying data fusion techniques that integrate data from multiple sources (Mahmood et al., 2012). Recent studies have used tractor-mounted visible and near-infrared (vis-NIR) spectroscopy to estimate various soil properties, such as soil moisture (SM), organic carbon, pH, electrical conductivity, and nutrients other than SMN. By combining proximal sensor data, topographic variables, and remotely sensed imagery, it was possible to successfully develop MZ and variable-rate fertilization recommendations (Guerrero et al., 2021b; J. Zhang et al., 2021). Though satellite imageries have been used to create MZ, the effectiveness of the zoning depends on the timing of the image acquisition, the spatial resolution of the imagery, the size of the fields, as well as the available ancillary

26396696, 2025, 1, Downloaded from https://acsess.onlinelibrary.wiley.com/doi/10.1002/agg2.70051 by Leibniz Institut Für Agrarlandschaftsforschung (Zalf) e., Wiley Online Library on [25/02/2025]. See the Terms and Conditions (https://onlinelibrary.wiley.com/terms-and-conditions) on Wiley Online Library for rules of use; OA articles are governed by the applicable Creative Commons License

26396696, 2025, 1, Downloaded from https://access.onlinelibrary.wiley.com/doi/10.1002/agg2.70051 by Leibniz Institut Für Agrarlandschaftsforschung (Zalf) e., Wiley Online Library on [25/02/2025]. See the Terms and Conditions (https://onlinelibrary.wiley.com/terms-and-conditions) on Wiley Online Library for rules of use; OA articles are governed by the applicable Creative Commons License

data (soil and topographic variables) (Breunig et al., 2020; Georgi et al., 2018; Javadi et al., 2022). In recent years, high-resolution 3-m multispectral imagery from PlanetScope has been used to determine the aboveground biomass of crops to delineate MZ. It was demonstrated that 3-m imagery could be an alternative between very high-resolution submeter pixel unmanned aerial vehicle and moderate resolution (30 m) Landsat imagery for fields cultivated with cereals (Breunig et al., 2020). Furthermore, a study conducted by Zhao et al. (2020) showed that vegetation indices such as normalized difference vegetation index (NDVI) and normalized difference red-edge index (NDRE) derived from the near-infrared (NIR) and red-edge (RE) bands of a handheld proximal sensor exhibited a negative correlation between nitrate leaching and the aboveground biomass or N content of cover crops. This finding underscores the potential for utilizing satellite imagery incorporating NIR and RE bands to monitor the spatio-temporal variability of NO_3^- at the field scale. In addition, data analysis methods such as principal component analysis, regression modeling, and *k*-means clustering have shown their suitability to combine information from diverse sources to identify patterns to create MZ (Mahmood et al., 2012; Nogueira Martins et al., 2020). However, it is important to note that these studies did not consider SMN and its fractions, highlighting a significant knowledge gap in this area.

Hence, despite the advancement in proximal and remote sensing applications, existing literature indicates a lack of studies on real-time in-field estimation of NO_3^- and SMN and thus the understudied possibility to delineate MZ based on in-season NO_3^-, SMN, and multisensory data fusion. This gap is primarily due to the dynamic nature of SMN, NO_3^-, and SM, as well as challenges associated with the portability of current sensors (Guerrero et al., 2021a). Amid this, a handheld portable device called FarmLab has recently been introduced, which utilizes impedance measurements and spectral analysis, ranging from UV to NIR, to estimate different N forms in the soil, especially NO_3^-, SMN, and SM across different soil types (sand, sandy loam, and loamy sand) (Vikuk et al., 2024). Successful evaluation and application of such a handheld device, combined with high-resolution satellite imagery, offers a novel approach to monitor soil nitrogen during critical crop stages. It holds the potential to reduce labor and costs, improve yields through tailored nitrogen applications, and promote sustainability by minimizing nitrogen leaching. With the increasing affordability and ease of use of precision tools, widespread adoption by farmers is likely in the near future. Given these challenges and opportunities, this study has two objectives: first, to assess the suitability of capturing the within-field spatial variability of SMN, NO_3^-, and SM using different methods (FarmLab and laboratory); second, to explore the potential of FarmLab data for creating soil MZ for spring fertilizer application in winter crops by integrating proximal sensor data, lab-based soil N data, topography, and high-resolution satellite imagery.

Core Ideas

- The study evaluated proximal soil sensing and data fusion to delineate management zones using in-season SMN, nitrate, soil moisture, topographic, and remote sensing inputs.
- Eleven data fusion combinations demonstrated time- and crop-dependent optimal clustering, integrating proximal, topographic, and remote sensing data.
- This novel approach can be scaled to farm and landscape scale, allowing farmers to leverage proximal and remote sensing data for in-season soil mineral nitrogen monitoring.

2 | MATERIALS AND METHODS

2.1 | Study area

The study site is located near Müncheberg in Brandenburg, Northeastern Germany (52°26.827′ N, 14°1492′ E). The studied fields are part of the patchCROP landscape laboratory and are owned and managed by a commercial farm (Grahmann et al., 2024). The landscape formed during the last glacial periods, rendering it a distinct hummocky ground moraine. Predominantly, the area showcases moraine terrains from recent epochs, with primary soil compositions from sandy loam to loamy sand derived from glacial sediments. Erosional and depositional activities have created a heterogeneous landscape in the designated study area (Deumlich et al., 2018; Koch et al., 2023). The elevation in the study area varies, with altitudes spanning from 61.6 to 87.9 m above sea level from east to west (GeoBasis-DE/LGB, 2023). On a 30-year average (January 1992 to December 2022), the observed mean monthly precipitation fluctuates between 36 and 76 mm, and the monthly average temperature varies from 0.3°C to 19.0°C (DWD weather station in Müncheberg at a 10 km distance to the study site, Figure 1a). Weather data of 15 min resolution for the study area were obtained from two weather stations at the eastern and western ends of the patchCROP field (Figure 1b), located less than 1 km away from the studied fields.

2.2 | Sampling design

Within the described agricultural landscape, two fields were selected for this investigation in the cropping cycle 2022/23 (Figure 2). Field-A spans an area of 24.6 ha planted with winter rapeseed (*Brassica napus* L.), while Field-B covers 17.5 ha sown with winter barley (*Hordeum vulgare* L.). Both fields

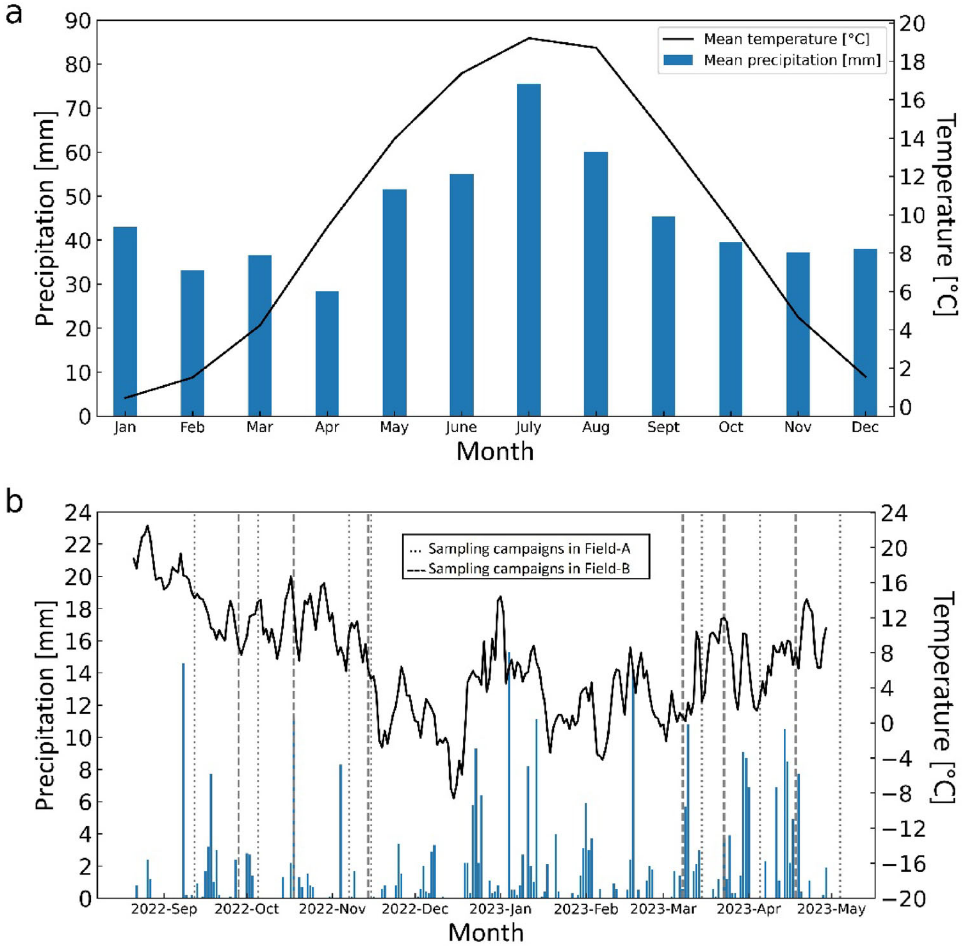

FIGURE 1 (a) The long-term mean monthly temperature and precipitation recorded at the Müncheberg weather station (1992–2022), (b) the daily precipitation and temperature during the study period at the study site, data were averaged from two weather stations at patchCROP (Figure 2); different vertical lines indicate the sampling dates in two fields (DWD Climate Data Center, 2023).

were under winter crop rotations with winter wheat (*Triticum aestivum* L.), barley, rapeseed, and cover crops (*Phacelia tanacetifolia* Benth.) and maize (*Zea mays* L.) (Table S1). The management data for both fields are presented in Tables S2 and S3 (historical fertilization only Field-A). A similar sampling scheme was implemented across both fields for comprehensive analysis. The design was intended to capture the maximum heterogeneity in SMN and SM during the early BBCH stage (Abd-Elmabod et al., 2017; Knowles & Dawson, 2018). The soil sampling grid was set at 130 m intervals to ensure systematic, representative sampling of each soil class while minimizing crop and soil disturbance. Repeated sampling at each location aimed to minimize crop disruption while maximizing temporal coverage. Soil data were derived from the German "Bodenschätzung" (scale 1:10,000), which is a soil map created in the 1930s and periodically updated (Figure 2). Although not consistently updated at the original 50 m × 50 m spatial resolution, the map provides detailed information on soil properties, including parent material, integrated soil texture to a depth of 1 m, and soil development stage (Eckelmann et al., 2005). The systematic sampling method involved collecting soil samples at the intersections of a predefined grid over the field, ensuring systematic and evenly spaced sampling points, and it led to a representative soil variability analysis across a large field. The selected configuration resulted in 14 sampling points in Field-A and 11 points in Field-B.

This study conducted simultaneous sampling campaigns to compare soil data using the FarmLab proximal soil sensor and manual soil sampling. The FarmLab device, as per its manufacturer, can estimate nitrate (NO_3^-), SMN, and SM up to 30 cm. However, preliminary trials showed that sampling at this depth during autumn, winter, and early spring caused significant crop disruption; hence, the sampling depth was adjusted to 20 cm. The soil surface was cleared of residues, roots, and stones before inserting the FarmLab into the soil (Figure 3). Three measurements were taken at each point, involving three punches within a close radius. Soils were manually sampled up to 20 cm depth using an auger within a 30–50 cm radius of each FarmLab

26396696, 2025, 1, Downloaded from https://acsess.onlinelibrary.wiley.com/doi/10.1002/agg2.70051 by Leibniz Institut Für Agrarlandschaftsforschung (Zalf) e., Wiley Online Library on [25/02/2025]. See the Terms and Conditions (https://onlinelibrary.wiley.com/terms-and-conditions) on Wiley Online Library for rules of use; OA articles are governed by the applicable Creative Commons License

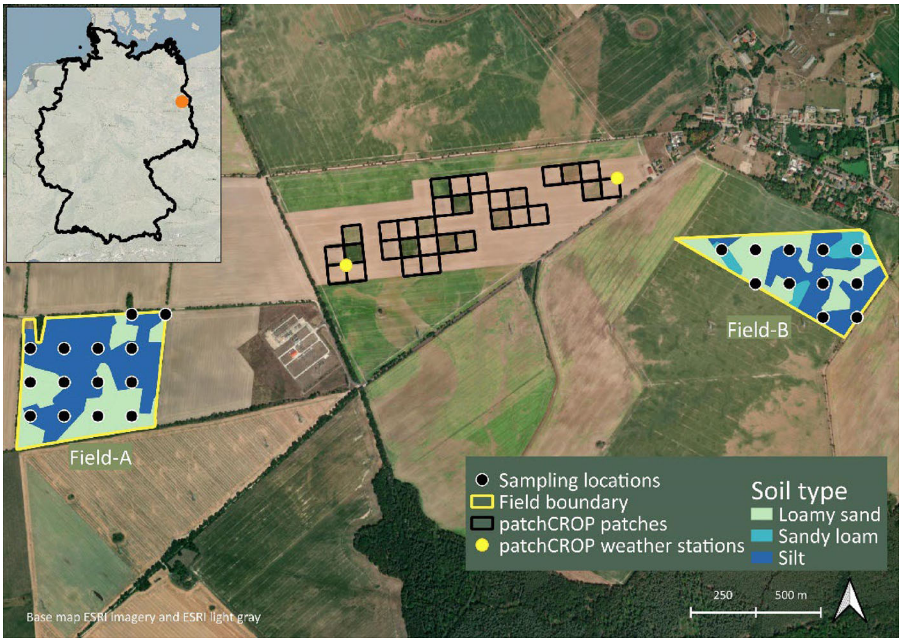

FIGURE 2 Location of fields, sampling points at the study site, and soil type information. Both fields are considered reference fields within the patchCROP landscape laboratory. Basemap: ESRI imagery and ESRI light gray.

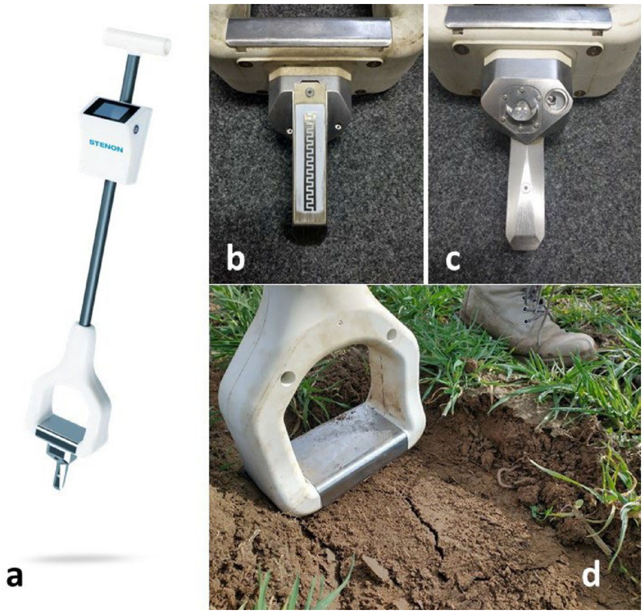

FIGURE 3 (a) FarmLab device, (b) electrode-based sensor, (c) visible and near-infrared (NIR)-based sensors, and (d) device punched inside the soil during a sampling campaign in March 2023. Image in (a) is adapted from https://stenon.io/; and images (b–d) are provided by authors.

measurement; three auger samples were collected to prepare one composite sample (see Figure S1). Field-A had 14 sampling points, and data were collected on seven dates, resulting in 98 measurements. Due to dense crop stands in Field-B, it was possible to sample six dates that provided 66 paired datasets from 11 points (Table S4). Sampling campaigns were paused during winter when the soil was frozen and on occasions when the soil was too dry (less than 5% SM at the beginning of May). In total, a dataset of 164 paired measurements was collected. The FarmLab device is equipped with ultraviolet-visible spectroscopy, NIR spectroscopy, electrochemical impedance spectroscopy sensors, global positioning system, light, temperature, and environmental sensors. The study used the software version rc-client-1.15.1 and the calibration model p-2.1.0 (Universal Unique Identifier: 6f10978b-3654-48fb-92fb-478b29e29c69). Further insights about this tool, including its intricate technological specifications and safety guidelines, can be found in the User Instructions (FarmLab—Stenon, 2024).

2.3 | Sample processing

Soil samples were promptly transported to the laboratory in cooling boxes. The concentration of NH_4^+-N and NO_3^--N from fresh soil was measured spectrophotometrically after extraction with a 0.1 M KCl solution using a continuous flow analyzer (Skalar Analytical B.V, CFA-SAN) according to DIN ISO 14256. SM was measured gravimetrically according to DIN ISO 11465, then converted to volumetric water content using an average bulk density of 1.65 g cm^{-3} as well as a depth of 20 cm. The certification documentation of FarmLab (German Agronomic Society, 2021) indicates that the device's standardization for NO_3^--N and SMN measurements was established using

26396696, 2025, 1, Downloaded from https://acsess.onlinelibrary.wiley.com/doi/10.1002/agg2.70051 by Leibniz Institut Für Agrarlandschaftsforschung (Zalf) e., Wiley Online Library on [25/02/2025]. See the Terms and Conditions (https://onlinelibrary.wiley.com/terms-and-conditions) on Wiley Online Library for rules of use; OA articles are governed by the applicable Creative Commons License

26396696, 2025, 1, Downloaded from https://access.onlinelibrary.wiley.com/doi/10.1002/agg2.70051 by Leibniz Institut Für Agrarlandschaftsforschung (Zalf) e., Wiley Online Library on [25/02/2025]. See the Terms and Conditions (https://onlinelibrary.wiley.com/terms-and-conditions) on Wiley Online Library for rules of use; OA articles are governed by the applicable Creative Commons License

TABLE 1 Spectral indices developed from the eight-band multispectral PlanetScope data.

Name of the index	Equation
Normalized difference vegetation index (NDVI)	$\frac{\text{NIR} - \text{red}}{\text{NIR} + \text{red}}$
Normalized difference red-edge index (NDRE)	$\frac{\text{NIR} - \text{red edge}}{\text{NIR} + \text{red edge}}$
Red-edge normalized difference index (RedEdge2)	$\frac{(\text{Red edge}-\text{red})}{(\text{Red edge}+\text{red})}$
Green normalized difference index (GNDVI-1 and GNDVI-2)	$\frac{\text{NIR} - \text{green}}{\text{NIR} + \text{green}}$
Ratio vegetation index (RVI)	$\frac{\text{NIR}}{\text{red}}, \frac{\text{red edge}}{\text{red}}, \frac{\text{NIR}}{\text{green}}, \frac{\text{NIR}}{\text{red edge}}$
Normalized difference red/green redness index (RI)	$\frac{(\text{Red}-\text{green})}{(\text{Red}+\text{green})}$
Difference vegetation index (DVI)	NIR − red
Leaf chlorophyll index (LCI)	$\frac{(\text{NIR}-\text{red edge})}{(\text{NIR}+\text{red})}$
Renormalized difference vegetation index (RDVI)	$\frac{(\text{NIR}-\text{red})}{\sqrt{(\text{NIR}+\text{red})}}$
Green–red normalized difference vegetation index (GRNDVI)	$\frac{\text{NIR}-(\text{green}+\text{red})}{\text{NIR}+(\text{green}+\text{red})}$

Note: All vegetation index equations were accessed through Index DataBase: A database for remote sensing indices (Henrich et al., 2012).

the reference method outlined in VDLUFA Vol. I, A6.1.4.1, an extraction method with calcium chloride ($CaCl_2$), and VDLUFA Vol. I, A2.1.1 for SM measurements. VDLUFA (Verband Deutscher Landwirtschaftlicher Untersuchungs- und Forschungsanstalten) standards are specific to German agricultural practices and are widely used in Germany's agricultural research and testing laboratories. However, due to the international usage of STENON, for example, in Brazil and Kazakhstan (https://blog.stenon.io/2024/08/12/stenon-news-for-agriculture-experts-july-august-2024/#more-2836), the widely accepted extraction procedure with KCl was chosen as the reference laboratory method (K. Li et al., 2012).

2.4 | Topographic and remote sensing variables

The digital elevation model (DEM) of 1 m spatial resolution was downloaded from GeoBasis-Deutschland (GeoBasis-DE/LGB, 2023), and slope and topographic wetness index were calculated from the DEM, using slope and aspect (Reddy, 2018). The PlanetLabs 8-band multispectral imagery with 3-m spatial resolution was collected via the German Federal Agency for Cartography and Geodesy (BKG) and was synchronized with the dates of the field sampling campaign (Table S4). The images were analytic ortho scene surface reflectance products with 0% cloud coverage over the study area. A series of indices were calculated using different band combinations (Table 1, Table S5). All calculated indices were numerously reported suitable (Zhao et al., 2020) for studying chlorophyll content and nitrogen in plants. Nitrogen status can vary spatially and temporally, and multiple indices can capture these variations more effectively than a single index (Xue & Su, 2017). Two green bands are available in the satellite imagery, allowing multiple indices to be developed with different combinations of green bands.

2.5 | Descriptive statistics

Data normality was checked using the Shapiro–Wilk test for each of the three variables (i.e., SMN, NO_3^-, and SM) obtained through FarmLab and laboratory analysis. Wilcoxon rank-sum test was carried out to compare differences between paired measurements (Schoot & Miočević, 2020). All steps were performed within the Python Jupyter Notebook environment by deploying the Python libraries pandas, numpy, scipy, matplotlib, and seaborn.

2.6 | Method comparison

A method comparison analysis was conducted to determine the degree of agreement between the two methodologies (FarmLab and laboratory). Since the laboratory method provides direct measurements and the proximal sensor offers estimates, it was essential to assess the level of agreement between the two approaches. Bland–Altman plots were used to visualize the difference (in measurement units) between two paired measurements on the y-axis and the average on the x-axis. The horizontal lines at the top and bottom of the plot showed a mean difference of ± 2 standard deviations. The wider the lines spread, the greater the variability in the difference, or in other words, the lesser the agreement between the measurements obtained with both methods (Bland & Altman, 1999; Grahmann et al., 2023).

2.7 | Management zone delineation

Despite spatial limitations in the experimental design, that is, grid size, we collected multitemporal data from fixed locations. In this study, inverse distance weighting interpolation with power parameters 2, 4, 6, 8, and 10 was applied,

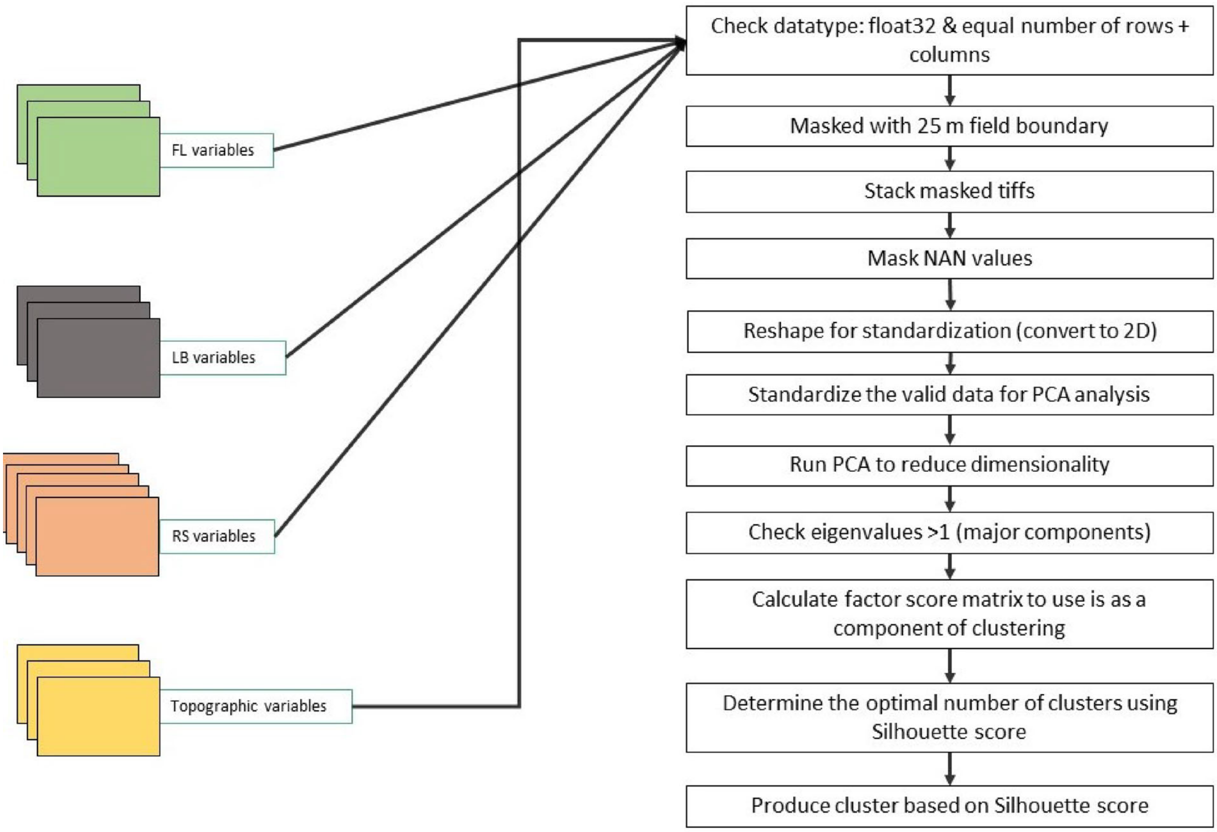

FIGURE 4 A simplified overview of k-means clustering steps followed in this study. This is an example of the model where all available feature sets (FL: FarmLab, LB: Laboratory, RS: remote sensing from planet image and topographic variables) were used to produce an optimal number of clusters or zones within the study area. PCA, principal component analysis.

generating 3-m spatial rasters (Guarneri & Weih, 2012), followed by the method described in Nawar (Nawar et al., 2017). The optimal raster data for each variable were identified using root mean squared error and mean absolute error. Spearman correlation examined collinearity among FarmLab-derived, laboratory, topographic, and remote sensing variables (Mezera et al., 2022). A multi-source data fusion approach was applied to delineate MZ within each field, integrating FarmLab (FL), lab results (LB), satellite imagery (RS), and topographic variables (TV). *K*-means clustering was applied to group similar data cells (Nogueira Martins et al., 2020), with 11 combinations of information layers to produce MZ (Figure S2). Two sampling dates per field were selected based on farmer's feedback and the common regulated fertilization scheme in Germany for winter crops: November 7, 2022, and March 15, 2023 for Field-A, and November 14, 2022, and March 8, 2023 for Field-B (Table S4).

K-means clustering was chosen for its computational efficiency and ability to handle large datasets with continuous variables. Unlike other methods (hierarchical clustering or fuzzy c-means), *k*-means is scalable to high-dimensional data and allows the user to test different combinations of layers (Capó et al., 2020). The clustering workflow involved the preprocessing of data before *k*-means was applied (Figure 4). Rasters were checked for consistency, co-registered, masked with a 25-m buffer, stacked, and filtered for NAN (Not a Number) values. The NAN values were mostly produced during the co-registration of different raster layers as well as due to the different raster extents of interpolated point data, topographic variables, and remote sensing imageries. However, it did not affect the clustering results because NAN values were masked with a 25-m buffer around the field edges. Principal component analysis (PCA) addressed multicollinearity, retaining components with eigenvalues >1 (Oldoni et al., 2019). The silhouette score is useful to determine the optimal number of clusters (k) in k-means clustering. By calculating the silhouette score for various numbers of k, the k with the highest average silhouette score can be chosen. This indicates clustering where data points are well-separated within their assigned clusters, ensuring robust and meaningful grouping (Mahi et al., 2018). Cluster labels were assigned based on ascending mean values. For each field and date, 11 k-means clustering outputs were produced.

As both fields were uniformly fertilized in spring 2023, end-of-season yield data, collected from two CLAAS Lexion 8700 TT harvesters, was used to validate the clustering

26396696, 2025, 1, Downloaded from https://acsess.onlinelibrary.wiley.com/doi/10.1002/agg2.70051 by Leibniz Institut Für Agrarlandschaftsforschung (Zalf) e., Wiley Online Library on [25/02/2025]. See the Terms and Conditions (https://onlinelibrary.wiley.com/terms-and-conditions) on Wiley Online Library for rules of use; OA articles are governed by the applicable Creative Commons License

TABLE 2 Descriptive statistics of the soil variables determined by FarmLab (FL) and laboratory analysis (LB).

Field	Variables	Mean	Median	Min	Max	SD	CV (%)	*W*
A	FL_NO_3^- (mg kg^{-1})	11.57	11.92	0.00	25.96	7.66	66.22	0.94**
	FL_SMN (mg kg^{-1})	13.69	12.70	4.40	25.96	5.49	40.14	0.94**
	FL_SM (%)	11.79	11.43	8.72	15.73	1.97	16.67	0.95**
	LB_NO_3^- (mg kg^{-1})	5.07	2.82	0.86	36.23	6.07	119.73	0.60**
	LB_SMN (mg kg^{-1})	11.63	7.96	1.75	64.01	11.33	97.40	0.73**
	LB_SM (%)	11.86	10.81	7.47	19.22	3.03	25.53	0.87**
B	FL_NO_3^- (mg kg^{-1})	9.65	7.76	0.00	24.12	7.78	80.68	0.89**
	FL_SMN (mg kg^{-1})	14.90	12.10	4.18	38.61	7.76	52.06	0.89**
	FL_SM (%)	12.47	12.60	7.96	17.03	2.66	21.32	0.94**
	LB_NO_3^- (mg kg^{-1})	3.51	1.62	0.11	53.11	8.10	230.68	0.35**
	LB_SMN (mg kg^{-1})	7.50	4.39	2.16	67.44	10.35	138.03	0.45**
	LB_SM (%)	12.44	12.55	4.40	20.40	4.26	34.29	0.95**

Note: FL_NO_3^- = NO_3^- from FarmLab, FL_SMN- = soil mineral N from FarmLab, FL_SM = soil moisture from FarmLab, LB_NO_3^- = NO_3^- from laboratory analysis, LB_SMN- = soil mineral N from laboratory, LB_SM = soil moisture from laboratory, Min = minimum, Max = maximum, SD = Standard deviation, CV = coefficient of variation, *W* = Shapiro–Wilk test of normality.
**$p < 0.05$.

outputs (Table S2). Yield map data were calibrated, standardized, and error-corrected (Donat et al., 2022; Maldaner et al., 2016), and yield clusters were derived using the silhouette method. The clustered yield grid was used to calculate the confusion matrix, kappa score, and mean squared error (MSE) to compare MZ results (Nogueira Martins et al., 2020). The kappa score assesses the agreement between categorical datasets, adjusting for chance agreement, while MSE evaluates model performance by averaging squared prediction errors. Python libraries (numpy, geopandas, scikit-learn, rasterio, pykrige fiona, and matplotlib) were used within a Jupyter Notebook environment to complete the procedure.

3 | RESULTS

3.1 | Nitrate, soil mineral nitrogen, and soil moisture

In Field-A, a significant difference ($p < 0.05$) was observed between the mean NO_3^- concentration estimated by FarmLab (FL; 11.57 mg kg^{-1}) and the laboratory method (LB; 5.07 mg kg^{-1}) (Tables 2 and 3). Similarly, for SMN, FL estimated a mean of 13.69 mg kg^{-1} compared to 11.63 mg kg^{-1} obtained by LB, indicating a significant difference ($p < 0.05$). SM showed a similar mean value (FL: 11.79%, LB: 11.86%) and was not significantly different ($p = 0.29$) (Tables 2 and 3). In Field-B, a significant difference ($p < 0.05$) was observed between the mean NO_3^- concentration estimated by FL (9.65 mg kg^{-1}) and LB (3.51 mg kg^{-1}) (Tables 2 and 3). For SMN, FL estimated a mean of 14.90 mg kg^{-1} compared to 7.50 mg kg^{-1} by LB, being significantly different ($p < 0.05$). SM obtained similar mean values (12.47% by FL and 12.44% by LB; $p = 0.77$) (Tables 2 and 3). A high coefficient of variation (%) derived from LB measured for NO_3^- and SMN indicated a higher variability of minimum and maximum values compared to FL (Table 2).

TABLE 3 Results of Wilcoxon rank-sum test for paired comparison of measured variables.

Field	Comparison	Test statistic	*p*-value
A	FL_SMN vs. LB_SMN	4.51	<0.05
	FL_NO_3^- vs. LB_NO_3^-	5.61	<0.05
	FL_SM vs. LB_SM	1.06	0.29
B	FL_SMN vs. LB_SMN	7.41	<0.05
	FL_NO_3^- vs. LB_NO_3^-	5.32	<0.05
	FL_SM vs. LB_SM	−0.29	0.77

Note: FL_NO_3^- = NO_3^- from FarmLab, FL_SMN = soil mineral N from FarmLab, FL_SM = soil moisture from FarmLab, LB_NO_3^- = NO_3^- from laboratory analysis, LB_SMN = soil mineral N from laboratory, LB_SM = soil moisture from laboratory.

A high deviation of SMN was observed in Field-A on a particular date, April 5, 2023. LB obtained a maximum SMN value of 64.01 mg kg^{-1}, while FL recorded only 22.9 mg kg^{-1} on that day for the same field (Figure 5). Data were collected 8 days after spring fertilization on March 28, 2023 (Table S2). Likewise, LB in Field-B measured a maximum SMN value of 67.43 mg kg^{-1} and a mean of 21.03 mg kg^{-1} on March 8, 2023, while FL estimated a maximum of 13 mg kg^{-1} and a mean of 8.49 mg kg^{-1}. The sampling was carried out 5 days after fertilization on March 3, 2023. Overall, an opposite trend was observed at the beginning and end of the sampling campaign, with NO_3^- and SMN values obtained by FarmLab being higher than those obtained in the

26396696, 2025, 1, Downloaded from https://acsess.onlinelibrary.wiley.com/doi/10.1002/agg2.70051 by Leibniz Institut Für Agrarlandschaftsforschung (Zalf) e., Wiley Online Library on [25/02/2025]. See the Terms and Conditions (https://onlinelibrary.wiley.com/terms-and-conditions) on Wiley Online Library for rules of use; OA articles are governed by the applicable Creative Commons License

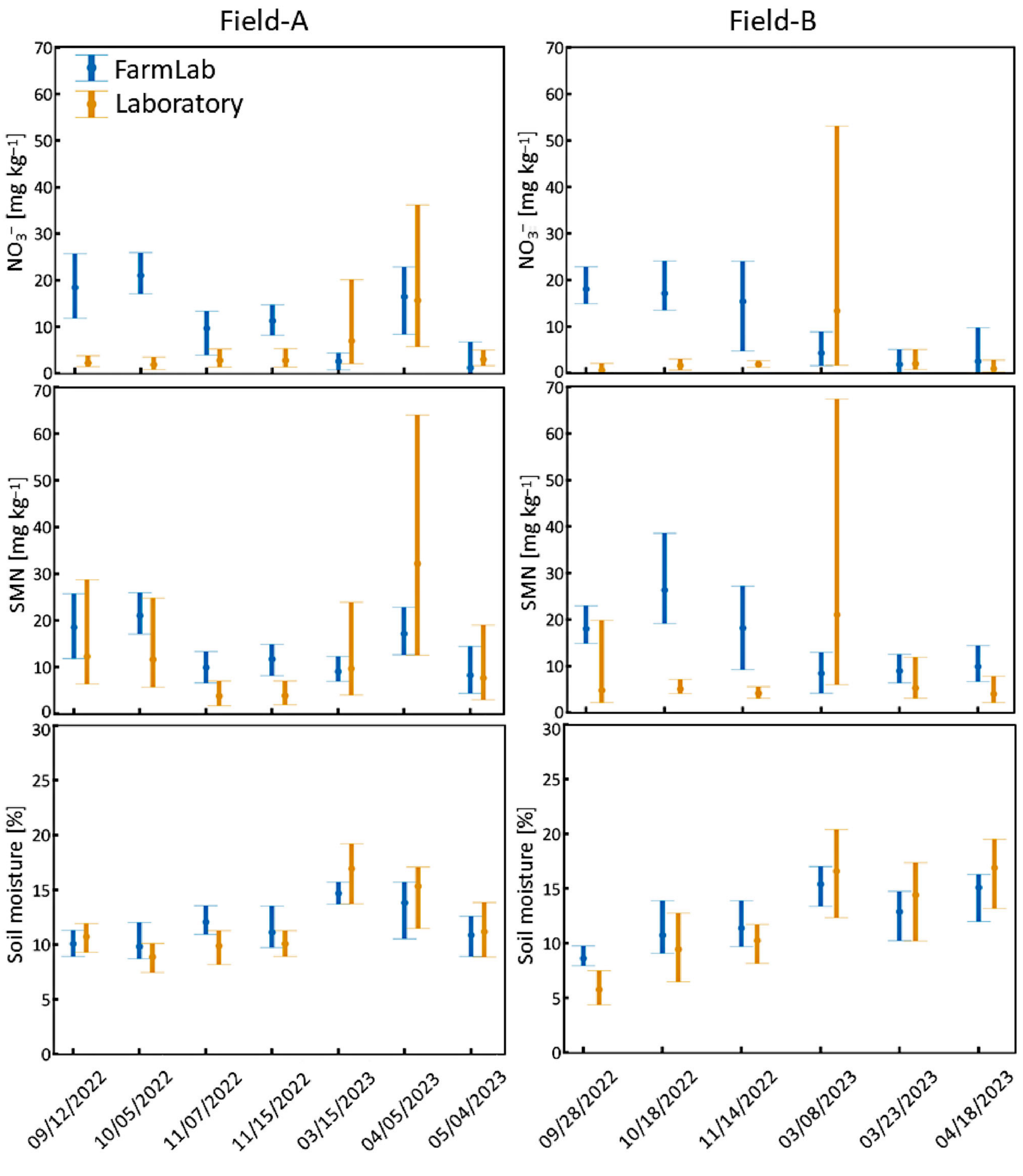

FIGURE 5 The mean values per field from individual sampling dates for NO_3^-, soil mineral nitrogen (SMN), and soil moisture derived by FarmLab and laboratory analysis; the left panel designates Field-A, and the right panel designates Field-B. The error bars are the actual minimum and maximum values observed per field on that specific sampling date.

laboratory and vice versa (Figure 5). Significant differences between FarmLab and laboratory were observed in Field-A for NO_3^- on six of seven dates and for SMN on five of seven dates ($p < 0.05$) (Table S6). In Field-B, SMN showed significant differences on five of six dates and for NO_3^- on three of six dates ($p < 0.05$) (Table S6).

3.2 | Bland–Altman plots for method agreement

The mean difference in NO_3^- obtained by FL and LB was more than 6 mg kg^{-1} for both fields (Figure 6a,b), and the limits of agreement were large in Field-B (−17.40 to 29.66 mg

26396696, 2025, 1, Downloaded from https://acsess.onlinelibrary.wiley.com/doi/10.1002/agg2.70051 by Leibniz Institut Für Agrarlandschaftsforschung (Zalf) e., Wiley Online Library on [25/02/2025]. See the Terms and Conditions (https://onlinelibrary.wiley.com/terms-and-conditions) on Wiley Online Library for rules of use; OA articles are governed by the applicable Creative Commons License

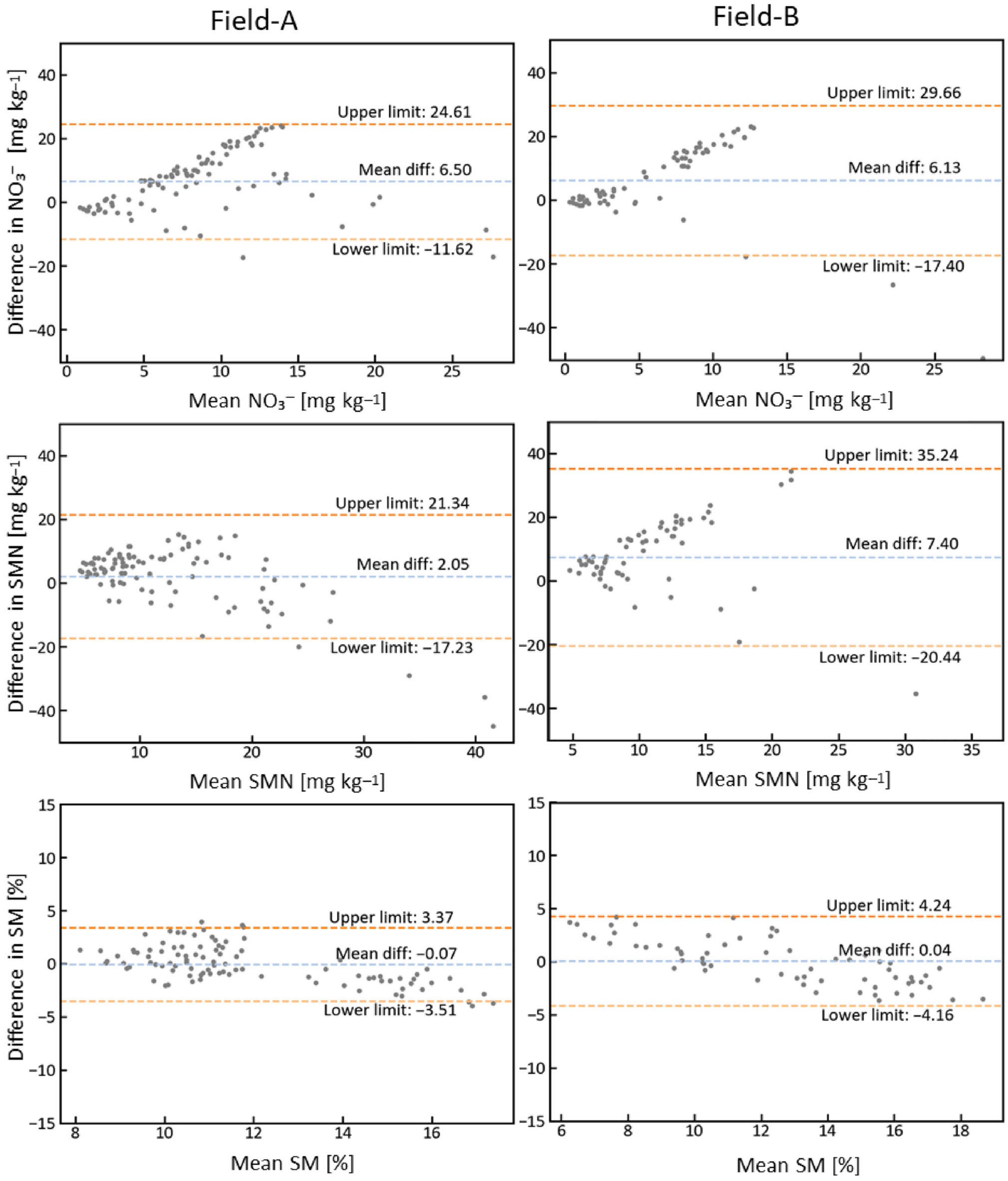

FIGURE 6 Bland–Altman plots for three variables determined in two fields. The left panel designates Field-A, and the right panel designates Field-B. The blue line indicates the mean difference between the two measurements, and the orange lines indicate the upper and lower limits of agreements between the two methods. SM, soil moisture; SMN, soil mineral nitrogen.

26396696, 2025, 1, Downloaded from https://acsess.onlinelibrary.wiley.com/doi/10.1002/agg2.70051 by Leibniz Institut Für Agrarlandschaftsforschung (Zalf) e., Wiley Online Library on [25/02/2025]. See the Terms and Conditions (https://onlinelibrary.wiley.com/terms-and-conditions) on Wiley Online Library for rules of use; OA articles are governed by the applicable Creative Commons License

kg^{-1}). The mean difference of SMN in Field-A was 2.05 mg kg^{-1}, compared to 7.40 mg kg^{-1} in Field-B (Figure 6c,d). Field-A showed a relatively satisfactory agreement with a narrower spread in the upper and lower limits, indicating greater agreement between the methods compared to Field-B. SM showed a negligible mean difference, suggesting little systematic difference between FL and LB (Figure 6e,f).

3.3 | Delineation of management zones

Results of Spearman correlation matrices for both fields showed FL NO_3^- and SMN had a positive correlation with single-band spectral values from satellite imagery, while most calculated indices showed negative correlations (Figure S3). SM measured with FL and LB correlated significantly and positively with the indices in Field-B; however, an insignificant correlation was observed in Field-A. Topographic variables did not correlate significantly with any FL, LB, or remote sensing variables. These findings also indicate multicollinearity among variables, which requires a PCA before applying the k-means clustering approach. Furthermore, Figure 7 illustrates eigenvalues >1 and the corresponding explained variance ratios of principal components (PCs) for different fields and dates, reflecting the variability across various feature set combinations. The first two PCs consistently captured most of the variance across both fields and dates (Figure 7a–d).

In both fields, feature sets with FarmLab (A) and laboratory (B) data, the eigenvalues of the first principal component (PC1) were relatively low and consistently below 4. In contrast, the eigenvalues for the remote sensing dataset (C) were between 13 and 14. Despite the lower eigenvalues in feature sets A and B, PC1 explained a substantial portion of the variance, which was between 65% and 90%. In contrast, feature sets incorporating remote sensing data (C) explained less than 60% of the variance. When topographical variables were included in the feature sets alongside FarmLab and laboratory data, the variance explained by PC1 dropped to less than 50%.

The silhouette score (Table 4) for selecting the optimal number of clusters showed that feature set B consistently achieved higher silhouette scores on three out of four dates, suggesting the presence of natural variability in the data. Additionally, feature set A from Field-B yielded the highest score on March 8, 2023, reflected in greater class separability and increased spatial variability in the data compared to all other feature sets. However, when multiple data were fused in the feature sets (e.g., A + C and A + C + D), it tended to show lower silhouette scores, suggesting that additional variables might introduce complexity, thus reducing class separability across different fields and dates. Overall, most feature sets showed two classes irrespective of fields and dates.

In both fields, *k*-means clustering results showed the creation of at least two zones, especially when remote sensing data were included (Figures 8 and 9). In Field-A, clustering based on autumn data (November 2022) using LB (feature set B) resulted in three clusters. However, in spring (March 2023), when FL data (feature set A) were utilized, up to nine clusters were identified, indicating a higher level of spatial variability during this period. Conversely, in Field-B, the autumn clustering results using FL data (feature set A) generated up to four clusters, whereas feature set (A + D) incorporating laboratory and topographic variables produced six clusters. In spring, both FL and LB data resulted in the formation of only two clusters, suggesting a reduced within-field spatial variability of the variables considered for clustering during this season.

MZ clusters of 11 feature sets (data fusion combinations) were evaluated against yield map data using Kappa score and MSE values (Table 5). In Field-A, the feature set combining FL and topographic variables resulted in the lowest MSE and an improved kappa score in November. The best performance was observed in March, when LB and topographic variables were combined (feature set A + D). In Field-B, despite a lower kappa score in November (0.135), there was a noteworthy improvement in March (0.436), with remote sensing variables incorporated in the analysis for both periods. Overall, the results showed that the inclusion of topographic variables provided the best fitting outputs irrespective of fields and dates (Figure 10).

4 | DISCUSSION

4.1 | Comparison between FarmLab and laboratory analysis

Developing a proximal sensor for direct estimation of NO_3^-, SMN, and SM in the field involves critical factors such as sensitivity and practicality (Guerrero et al., 2021a). In this context, the present study examined the feasibility of using FarmLab as an alternative to traditional laboratory methods to assess spatial variability of nitrogen at the field scale. Although the primary focus was not a quantitative comparison of the two methods, the study also explored the underlying causes for the discrepancies observed between the FarmLab proximal sensor and laboratory measurements. The maximum values of NO_3^- and SMN determined by FarmLab were within the specified threshold mentioned by the FarmLab manufacturer (40 and 45 mg kg^{-1} for NO_3^- and SMN, respectively) (German Agronomic Society, 2021). SM also followed the 5% to <25% threshold, which indicated FarmLab's inherent limits to estimate a wide range of values. Furthermore, Bland–Altman plots showed dissimilarities in NO_3^- and SMN between the two methods (Figure 6), which

26396696, 2025, 1, Downloaded from https://acsess.onlinelibrary.wiley.com/doi/10.1002/agg2.70051 by Leibniz Institut Für Agrarlandschaftsforschung (Zalf) e., Wiley Online Library on [25/02/2025]. See the Terms and Conditions (https://onlinelibrary.wiley.com/terms-and-conditions) on Wiley Online Library for rules of use; OA articles are governed by the applicable Creative Commons License

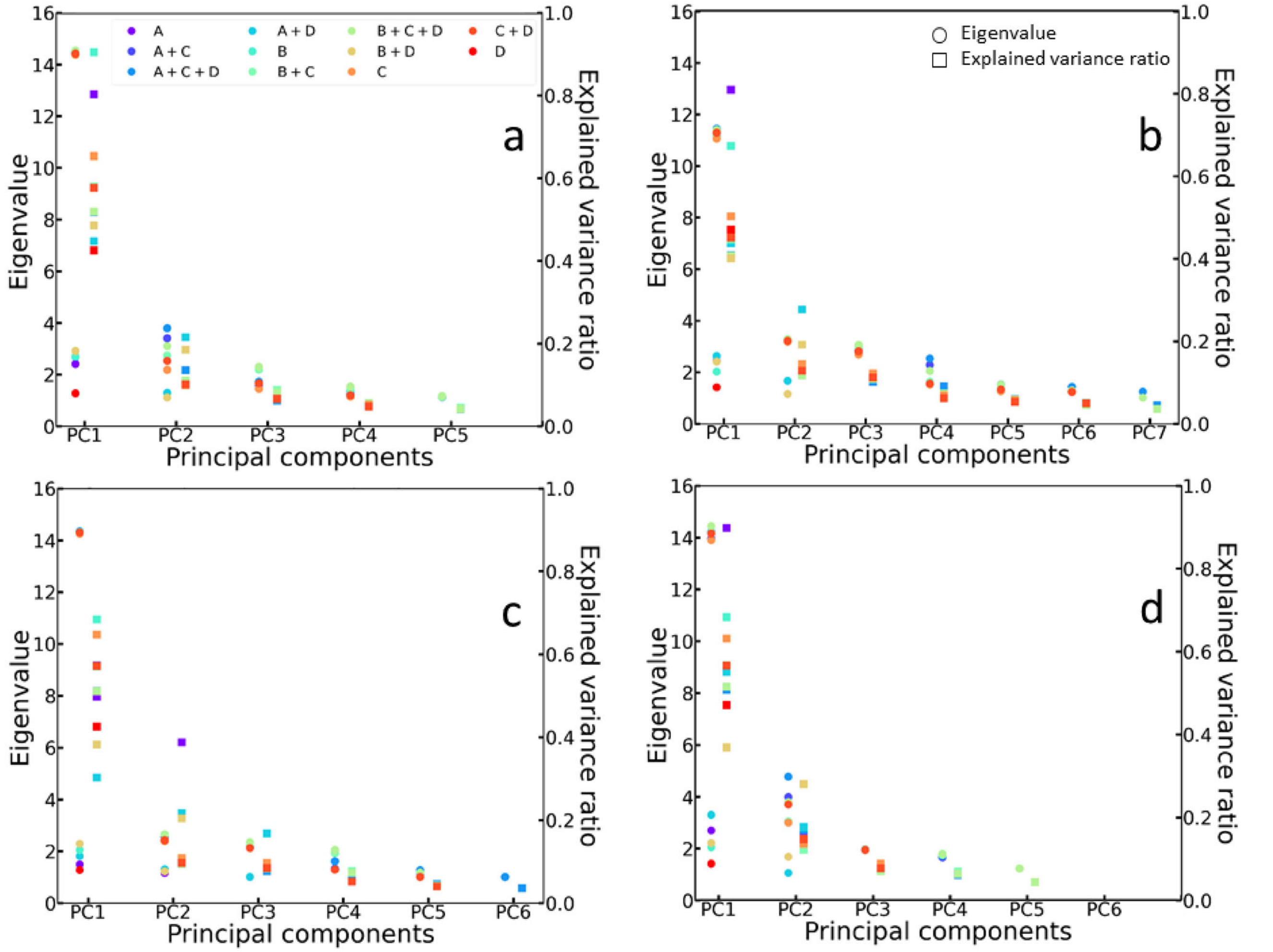

FIGURE 7 Principal component eigenvalues and explained variance ratios for different feature set combinations across fields and dates. Here, (a) Field-A November 7, 2022; (c) Field-A March 15, 2023; (b) Field-B November 14, 2022; and (d) March 08, 2023.The eigenvalues >1 are shown with dots (o), while explained variance ratios (right *y*-axis) are shown as squares (□). For each feature set, specific colors were selected to represent the eigenvalues and their corresponding variance ratio. A = FarmLab, B = Laboratory, C = Remote sensing, D = Topographic variables. Details on the variables are presented in Figures S2 and S3.

confirmed that FarmLab underestimated higher SMN values and overestimated lower ones compared to the laboratory method. A recent study by Vikuk et al. (2024) reported similar results, where the mean concentrations of NO_3^- and SMN measured in three different study areas were significantly higher with FarmLab than the laboratory ($p < 0.05$). In our study, both fields exhibited significant differences (NO_3^-, SMN) under heterogeneous soil textures, including loamy sand, sandy loam, and silt present in both fields (Figure 2). Although both studies (Vikuk et al., 2024, and the present study) were conducted on soil types recommended for FarmLab use—namely, sandy, silty, and loamy soils—the significant differences observed between the methods may be attributed to the higher proportion of sandy soils in our study area. Additionally, variations in sample processing, such as sieve size, type and amount of extracting solution, and the solution-to-soil ratio used by FarmLab, may have contributed to these discrepancies (German Agronomic Society, 2021; K. Li et al., 2012; Vikuk et al., 2024).

Another reason for the observed disagreement (Figure 6) between FarmLab and the laboratory method could be the extraction method followed in our study (KCl). Vikuk et al. (2024) also applied a similar extraction method as FarmLab's, being $CaCl_2$, and reported an under- and overestimation of more than 50 kg ha^{-1} SMN by FarmLab compared to the laboratory method. A study by K. Li et al. (2012) demonstrated that the concentrations of NO_3^- and NH_4^+ in soil were significantly higher when extracted with KCl compared to $CaCl_2$. Nevertheless, other factors such as extraction duration, storage time, and temperature can affect the extraction results (K. Li et al., 2012). In our study, although the extraction was performed with KCl, the mean concentration of NO_3^- and SMN measured by LB was lower for both fields compared to FarmLab estimates, which argues against the relevant

26396696, 2025, 1, Downloaded from https://acsess.onlinelibrary.wiley.com/doi/10.1002/agg2.70051 by Leibniz Institut Für Agrarlandschaftsforschung (Zalf) e., Wiley Online Library on [25/02/2025]. See the Terms and Conditions (https://onlinelibrary.wiley.com/terms-and-conditions) on Wiley Online Library for rules of use; OA articles are governed by the applicable Creative Commons License

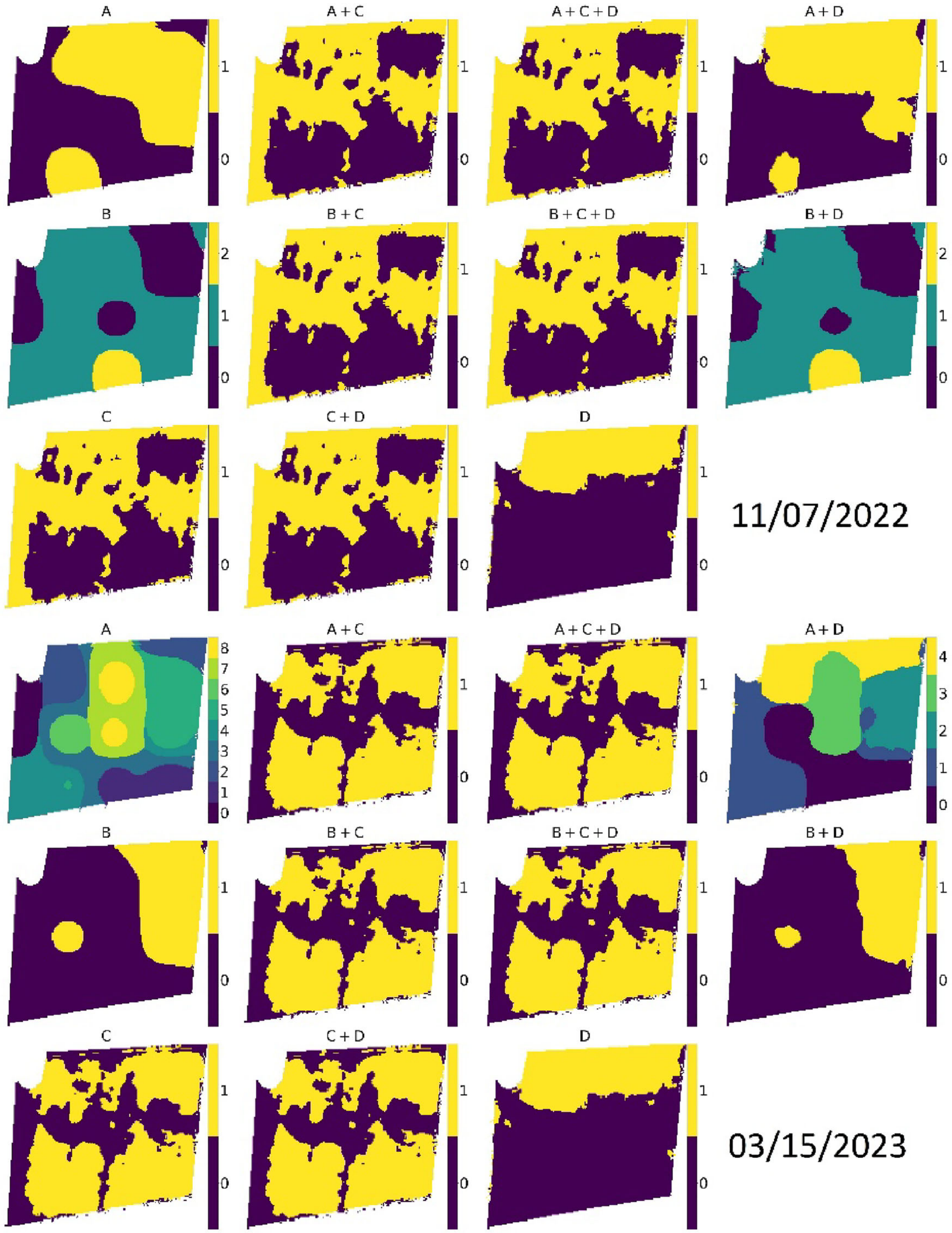

FIGURE 8 *K*-means clustering output using data from four different sources in 11 different feature sets in Field-A. The figure above shows results derived from data collected on November 7, 2022; the figure below represents data collected on March 15, 2023. The color legend on the right side of each plot indicates the number of clusters. A = FarmLab derived (NO_3^-, soil mineral nitrogen [SMN], and soil moisture [SM]), B = Laboratory derived (NO_3^-, SMN, and SM), C = remote sensing bands and derived indices, D = topographic variables (digital elevation model [DEM], slope, and topographic wetness index).

26396696, 2025, 1, Downloaded from https://acsess.onlinelibrary.wiley.com/doi/10.1002/agg2.70051 by Leibniz Institut Für Agrarlandschaftsforschung (Zalf) e., Wiley Online Library on [25/02/2025]. See the Terms and Conditions (https://onlinelibrary.wiley.com/terms-and-conditions) on Wiley Online Library for rules of use; OA articles are governed by the applicable Creative Commons License

TABLE 4 Silhouette scores and the optimal number of clusters for different data fusion combinations for two fields on multiple dates.

Field	Field-A				Field-B			
Date	November 7, 2022		March 15, 2023		November 14, 2022		March 8, 2023	
Feature sets	Silhouette score	Optimum cluster	Silhouette score	Optimum cluster	Silhouette score	Optimum cluster	Silhouette score	Optimum cluster
A	0.428	2	0.39	9	0.48	4	0.58	2
A + C	0.301	2	0.31	2	0.23	2	0.27	2
A + C + D	0.255	2	0.276	2	0.22	2	0.25	2
A + D	0.3	2	0.242	5	0.36	3	0.4	2
B	0.57	3	0.51	2	0.46	2	0.55	2
B + C	0.301	2	0.31	2	0.23	2	0.27	2
B + C + D	0.27	2	0.276	2	0.21	2	0.25	2
B + D	0.301	3	0.33	2	0.32	6	0.36	2
C	0.34	2	0.35	2	0.25	2	0.3	2
C + D	0.3	2	0.31	2	0.24	2	0.27	2
D	0.35	2	0.35	2	0.37	4	0.37	4

Note: A = FarmLab, B = Laboratory, C = Remote sensing, D = Topographic variables.

TABLE 5 Performance metrics (mean squared error [MSE] and Kappa score) for different feature sets across two fields (Field-A and Field-B) on two dates (November 7, 2022, and March 15, 2023, for Field-A, and November 14, 2022, and March 8, 2023, for Field-B).

Field	Field-A				Field-B			
Date	November 7, 2022		March 15, 2023		November 14, 2022		March 8, 2023	
Feature sets	MSE	Kappa score	MSE	Kappa score	MSE	Kappa score	MSE	Kappa score
A	0.342	0.269	18.102	0.000	2.493	0.147	0.301	−0.127
A + C	0.448	0.040	0.516	0.032	0.451	−0.025	0.217	0.421
A + C + D	0.448	0.036	0.517	0.033	0.453	−0.029	0.205	0.436
A + D	0.330	0.246	4.102	0.075	1.041	−0.007	0.293	−0.116
B	0.821	−0.104	0.168	0.512	0.393	−0.068	0.246	−0.070
B + C	0.444	0.048	0.674	0.072	0.462	0.136	0.293	0.397
B + C + D	0.445	0.049	0.516	0.038	0.457	−0.035	0.218	0.415
B + D	0.842	−0.094	0.158	0.522	6.912	0.179	0.209	0.105
C	0.646	0.088	0.675	0.072	0.459	0.138	0.286	0.405
C + D	0.647	0.088	0.518	0.036	0.456	0.135	0.270	0.427
D	0.330	0.034	0.330	0.034	3.123	0.155	3.123	0.155

Note: A = FarmLab, B = Laboratory, C = Remote sensing, D = Topographic variables. Gray-colored cells indicate the best fitting feature sets from specific dates for both fields.

role of the extraction method choice but underpins the importance to verify and calibrate sensor technologies not only in the national but also in the international context and usage applications (Liu et al., 2023). Previous studies using vis-NIR spectroscopy showed promising results in predicting NO_3^- levels in dried soils under a laboratory setting (Tsakiridis et al., 2017), while Guerrero et al. (2021a) confirmed that it was possible to successfully predict total nitrogen using the vis-NIR spectrum but not the mineral N fraction. Metzger and Bragazza (2024) used a handheld vis-NIR spectrophotometer and KCl extraction combined with Partial Least Squares Regression (PLSR) to analyze soil organic carbon (SOC), total nitrogen (N_{tot}), NO_3^- and NH_4^+ in clay soils. They achieved reliable predictions for N_{tot} and promising results for NO_3^- but found that predicting NH_4^+ was not possible due to its complex absorption properties related to soil cation exchange capacity.

A notable observation in our study are the differing correlations between SM and NO_3^-, as well as SMN (Figure S3a,b). In both fields, SM exhibited a negative correlation with NO_3^- and SMN when assessed by FL, in contrast to positive correlations observed with the laboratory method. A

26396696, 2025, 1, Downloaded from https://access.onlinelibrary.wiley.com/doi/10.1002/agg2.70051 by Leibniz Institut Für Agrarlandschaftsforschung (Zalf) e., Wiley Online Library on [25/02/2025]. See the Terms and Conditions (https://onlinelibrary.wiley.com/terms-and-conditions) on Wiley Online Library for rules of use; OA articles are governed by the applicable Creative Commons License

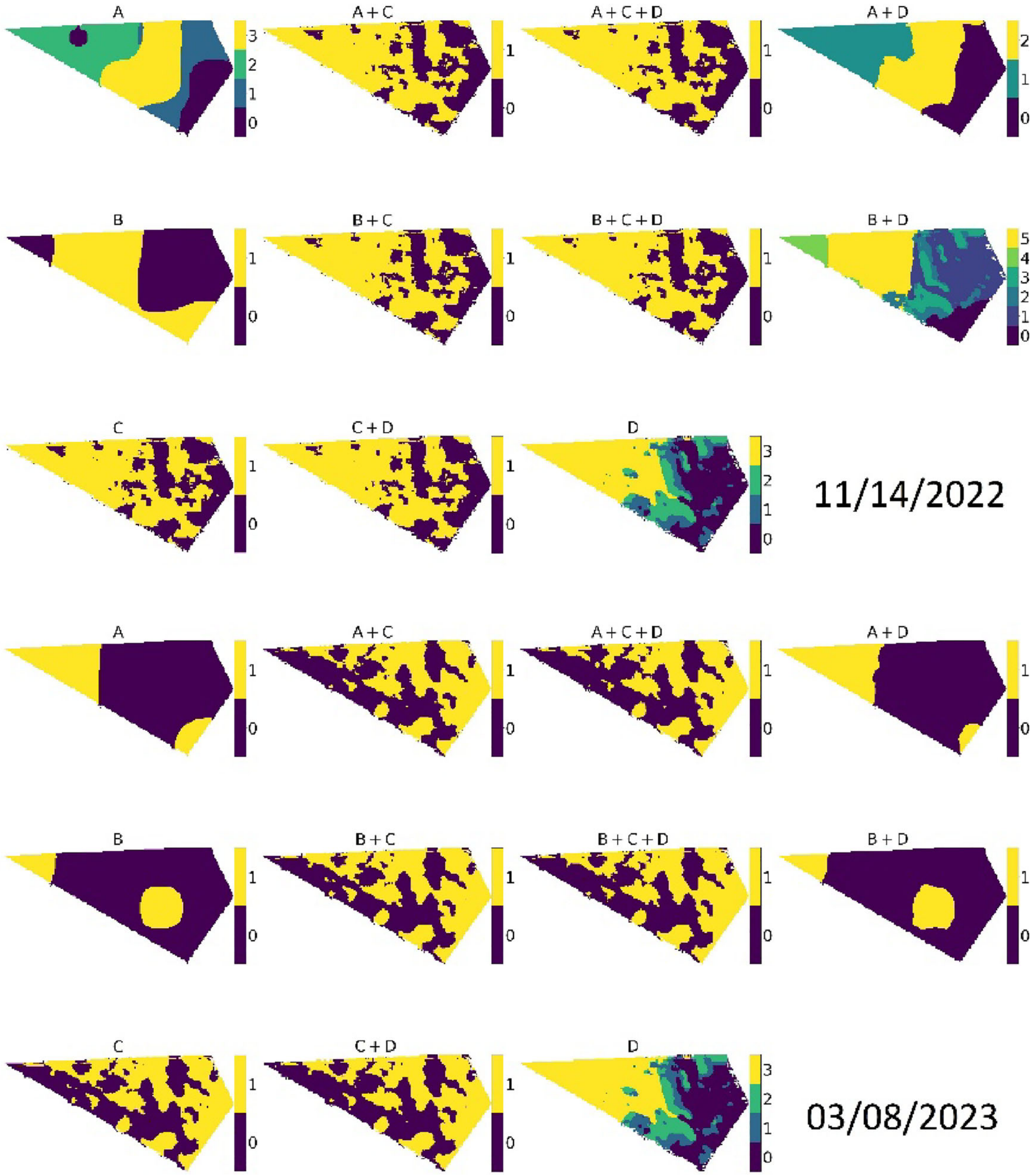

FIGURE 9 *K*-means clustering output using data from four different sources in 11 different feature sets in Field-B. The figure above shows results derived from data collected on November 14, 2022; the figure below represents data collected on March 8, 2023. The color legend on the right side of each plot indicates the number of clusters. A = FarmLab, B = Laboratory, C = Remote sensing, D = Topographic variables.

study by R. Zhang and Wienhold (2002) showed that NO_3^- positively correlated with SM up to 80% of water-filled pore space. The current study observed that for a range of 11%–20% SM in both fields, laboratory results showed a positive correlation among NO_3^- and SMN with SM. On the other hand, the negative correlation observed with FarmLab could be due to the type of sensor combination used or the calibration procedure followed by FarmLab. Although the SM measured by both methods showed similar trends, SM data did not contribute to understand the differences in mineral N dynamics by both methods. The exact reasons for the differences between FarmLab and laboratory results have not been elucidated in this study as the specific regression or calibration models used by FarmLab for estimating NO_3^-, SMN, and SM are protected by commercial patents. Despite these limitations, FarmLab's practical utility lies in its ability to provide quick, field-based assessments, which can inform fertilizer management decisions with a reasonable understanding of its limitations. For example, while FarmLab's discrepancies from laboratory methods may lead to under- or overestimation of precise nitrogen levels, its real-time measurements allow farmers and agronomists to make timely decisions

26396696, 2025, 1, Downloaded from https://acsess.onlinelibrary.wiley.com/doi/10.1002/agg2.70051 by Leibniz Institut Für Agrarlandschaftsforschung (Zalf) e., Wiley Online Library on [25/02/2025]. See the Terms and Conditions (https://onlinelibrary.wiley.com/terms-and-conditions) on Wiley Online Library for rules of use; OA articles are governed by the applicable Creative Commons License

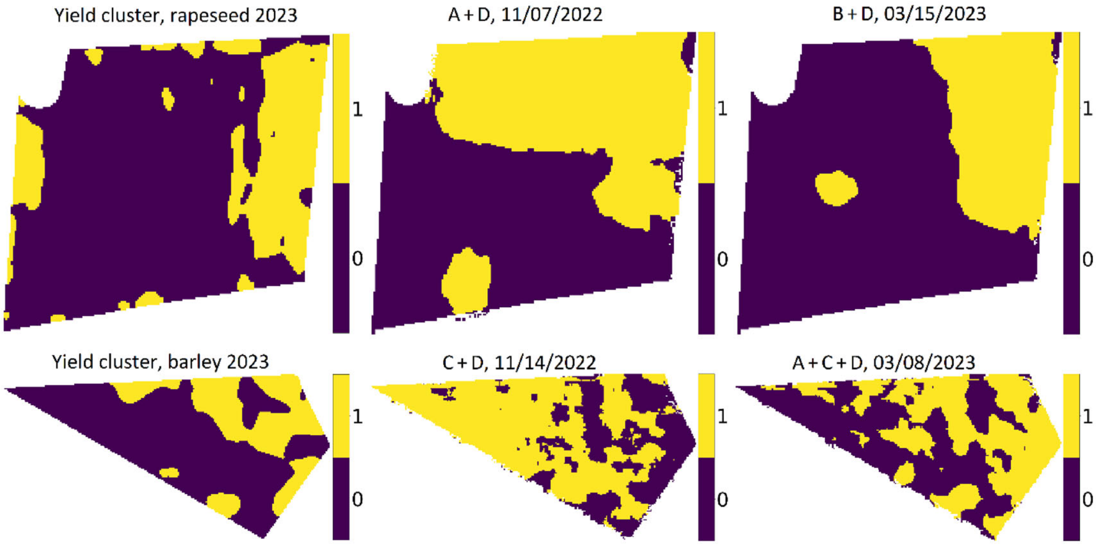

FIGURE 10 Yield cluster produced from combined harvester data and the best fitting feature sets on different dates. The upper row represents Field-A, the lower row depicts Field-B, A = FarmLab, B = Laboratory, C = Remote sensing, D = Topographic variables.

regarding the need of variable-rate fertilizer applications. This is particularly valuable during critical growth stages when laboratory results may not be immediately available. However, our results suggest that FarmLab's estimates may be more suited for within-field spatial variability assessment rather than precise nitrogen quantification. For specific crops or management practices, such as those requiring highly accurate nitrogen inputs, calibration against laboratory methods may be necessary to improve its reliability. Nonetheless, its portability and ease of use make FarmLab a practical tool for initial field assessments, particularly in resource-limited settings or when rapid decisions are needed.

4.2 | Implication of multisensory data fusion and delineation of management zones

Although the delineation of MZ is a well-established practice in precision agriculture (Guerrero et al., 2021a; Nawar et al., 2017), the integration of in-season data on NO_3^-, SMN, and the fusion of this information with remote sensing and topographic variables has not been thoroughly investigated in the existing literature. This study therefore introduces a novel approach by harnessing the capabilities of a handheld proximal sensor device and high-resolution satellite imagery, particularly during critical crop growth periods. The suitability of FarmLab, despite its limited agreement with laboratory-based results, was tested for its potential to combine remote sensing and topographic variables to delineate MZ, which in turn captures spatial variability. The methods approached in the current study can also be implemented further to track NO_3^--leaching hotspots within the fields and for spring fertilization of winter crops. Since nitrogen leaching typically occurs between September and April in temperate climates (Zhao et al., 2020), the correlation between remote sensing indices and FarmLab-derived NO_3^-, SMN, and SM could facilitate the identification of NO_3^- hotspots in the field. To enhance this approach, future studies could integrate crop biomass, plant nitrogen data, remote sensing imagery, and FarmLab measurements (Zhao et al., 2020).

Previous studies have demonstrated that the incorporation of topographic variables improves MZ delineation (Vallentin et al., 2020). In our analysis (Table 5, Figure 10), fusion of topographic variables with other data achieved the best fit for both fields, whereas feature sets relying solely on topographic data were less effective. A similar pattern was observed with remote sensing data; feature set C from both fields did not produce optimal MZ. In Field-A, remote sensing data alone did not improve MZ delineation, likely due to the timing of image acquisition during the BBCH 18 and BBCH 24 growth stages of rapeseed, resulting in low plant coverage and high soil reflectivity. In contrast, Field-B showed improved kappa scores for the feature set that included remote sensing variables during autumn and spring dates, suggesting better crop reflectance from barley compared to rapeseed (Table S7). Despite different spectral signatures and reflectance angles of barley and rapeseed (Kuester & Spengler, 2018), the higher NDRE and NDVI values (Table S7) from barley indicated that higher reflectance values from barley might have contributed to improved clustering results when integrating RS indices with FarmLab and topographic variables. Furthermore, one of the key advantages of using PlanetScope satellite imagery over freely available Sentinel-2 10-m imagery is the availability of two green bands at a 3-m resolution. When combined with NIR, these green bands contribute to monitor vegetation health and biomass production (Kharel et al., 2023). In the current study, PCA of the best fitting feature sets (A + C + D and C + D) for Field-B showed that the green–red

26396696, 2025, 1, Downloaded from https://acsess.onlinelibrary.wiley.com/doi/10.1002/agg2.70051 by Leibniz Institut Für Agrarlandschaftsforschung (Zalf) e., Wiley Online Library on [25/02/2025]. See the Terms and Conditions (https://onlinelibrary.wiley.com/terms-and-conditions) on Wiley Online Library for rules of use; OA articles are governed by the applicable Creative Commons License

normalized difference vegetation index (GRNDVI), calculated from the two green bands (bands 3 and 4), was the most contributed variable in the first principal component (PC1), followed by NDVI, renormalized difference vegetation index, and NDRE indices. This finding is particularly relevant given that several studies have reported that NDVI can be saturated depending on plant density, canopy cover, and growth stage (Gracia-Romero et al., 2023). In this context, alternative indices like GRNDVI could be more effective to capture variations in N-related crop conditions, providing a more nuanced understanding of vegetation health and N status of the crops that can also be translated into N leaching hotspots in the field (Zhao et al., 2020).

The current study applied unsupervised k-means clustering to multiple feature sets through silhouette score assessment and produced MZ. Feature sets derived from single-source data exhibited greater class separability, notably, soil variables from FarmLab in Field-B on March 8, 2023 (Table 4). The highest silhouette score from the FarmLab feature set in spring indicated FarmLab's potential as a quick tool to assess the spatial variability of N within the field. However, it also showed that the performance could be crop dependent. Furthermore, feature sets incorporating remote sensing data exhibited lower cluster separability in both fields on both dates; this outcome is likely attributed to remote sensing data's low spatial variability in the reflectance values. As remote sensing primarily detects aboveground nitrogen (N) or plant N status, MZ derived solely from remote sensing data (feature set C) were not optimal for either field or date. Nevertheless, feature sets that integrated remote sensing and topographic variables demonstrated best fitting clusters and emphasized the benefits of data fusion in delineating MZ for spring fertilization management.

The practical implications of these clustering results are significant for precision agriculture and overall farm management. Differences in clustering outcomes affect fertilizer application strategies by altering the number of identified zones with varying nutrient demands. For instance, integrating topographic and remote sensing variables led to more robust clustering, which allows farmers to optimize fertilizer application rates tailored to specific zones, potentially reducing overapplication and environmental impacts. However, the trade-offs between data complexity and clustering performance must also be considered in terms of field size, presence of permanent traffic lines, and available machinery (Donat et al., 2023). While multi-source data fusion improves clustering accuracy, it requires additional resources, such as high-resolution satellite imagery and proximal sensor devices, which may be cost-prohibitive for small-scale farmers (Kernecker et al., 2020). Simplified clustering approaches, using a limited number of variables like FL data alone, could be a practical alternative for resource-limited scenarios, as demonstrated by the high silhouette scores achieved with soil variables in Field-B. The methods presented in this study can be scaled up for larger farms and different crop types by tailoring the field sampling campaign and feature sets to specific field conditions and crop requirements.

Increasing the sampling density through a narrower grid design could potentially improve model precision. However, this approach proved impractical for the tested on-farm applications. The performance of FarmLab in our study was compromised by the presence of crop residues, which are common in fields managed under conservation agriculture where straw is retained on the surface postharvest. Additionally, the landscape's formation, characterized by a high prevalence of stones in the topsoil, further impeded FarmLab's functionality. As noted by Najdenko et al. (2024), the accuracy and performance of spectral sensors can be significantly influenced by soil surface conditions, tillage practices, and the presence of stones. In our case, these factors increased the time required to complete measurements, as it was challenging to obtain three consecutive error-free soil punches due to frequent interference from residues and stones. These challenges highlight the importance of considering field conditions when using spectral sensors. The current study did not include soil texture, organic carbon, or total nitrogen as additional comparable soil variables. Future studies may benefit from adding these variables estimated by FarmLab, which could offer valuable information on drivers for spatial and temporal mineral N dynamics (Guerrero et al., 2021a; Zhao et al., 2020).

5 | CONCLUSIONS

This study comprehensively tested a newly developed proximal sensor system as an alternative to field sampling and laboratory analysis for mineral N determination in the topsoil. Although the comparative analysis between the two methods did not result in a satisfactory agreement, the FarmLab data facilitated the capture of within-field variability and the delineation of MZ. The accuracy of the delineated MZ differed between the two cropped fields. Although rapeseed did not present consistent feature sets for practical use, remote sensing imagery combined with topographic and FarmLab variables proved effective for barley. This study highlights the challenges of evaluating in-season spatial variability of SMN and delineating MZ for different crops. Nevertheless, the results support the delineation of MZ with FarmLab as an additional data source, which may provide new opportunities for more inclusive and efficient fertilization management using multi-sensor and openly available datasets.

AUTHOR CONTRIBUTIONS

Md Tawhid Hossain: Conceptualization; data curation; formal analysis; investigation; methodology; writing—original draft. **Marco Donat**: Writing—review and editing. **Ines Astrid Tougma**: Writing—review and editing.

26396696, 2025, 1, Downloaded from https://acsess.onlinelibrary.wiley.com/doi/10.1002/agg2.70051 by Leibniz Institut Für Agrarlandschaftsforschung (Zalf) e., Wiley Online Library on [25/02/2025]. See the Terms and Conditions (https://onlinelibrary.wiley.com/terms-and-conditions) on Wiley Online Library for rules of use; OA articles are governed by the applicable Creative Commons License

Sonoko Bellingrath-Kimura: Supervision; writing—review and editing. **Kathrin Grahmann**: Conceptualization; funding acquisition; project administration; supervision; writing—review and editing.

ACKNOWLEDGMENTS

We thank the ZALF central laboratory for soil sample analysis. The German Federal Agency for Cartography and Geodesy (BKG) provided satellite imagery. We want to thank the collaborating farm, "Komturei Lietzen GmbH," for allowing us to use their fields for the experiment. We also thank the student assistants Igor Andin, Ayushi Joshi, Nouman Gulzar, and ZALF technical staff members Felix Erbe and Robert Zieciak for their support in the field and additional data collection. During the preparation of this work, we used ChatGPT and Ref-N-Write to improve the manuscript. After using these tools, we reviewed and edited the content as needed and take full responsibility for the content of the publication. This work was supported by the Leibniz-Centre for Agricultural Landscape Research (ZALF)-funded priority project "Optimal Nitrogen Supply for Future Agricultural Landscapes: digital technologies to optimize trade-offs." The maintenance of the patchCROP infrastructure is supported by the Leibniz Centre for Agricultural Landscape Research. Kathrin Grahmann acknowledges support from BMBF for the Junior Research Group SoilRob, project ID 031B1391.

Open access funding enabled and organized by Projekt DEAL.

CONFLICT OF INTEREST STATEMENT

The authors declare no conflicts of interest.

DATA AVAILABILITY STATEMENT

Data will be made available on request.

ORCID

Md Tawhid Hossain https://orcid.org/0000-0002-3563-2986

REFERENCES

Abd-Elmabod, S. K., Jordán, A., Fleskens, L., Phillips, J. D., Muñoz-Rojas, M., van der Ploeg, M., Anaya-Romero, M., El-Ashry, S., & de la Rosa, D. (2017). Chapter 7 - Modeling agricultural suitability along soil transects under current conditions and improved scenario of soil factors. In P. Pereira, E. C. Brevik, M. Muñoz-Rojas, & B. A. Miller (Eds.), *Soil mapping and process modeling for sustainable land use management* (pp. 193–219). Elsevier. https://doi.org/10.1016/B978-0-12-805200-6.00007-4

Ali, M. A., Wang, X., Chen, Y., Jiao, Y., Mahal, N. K., Moru, S., Castellano, M. J., Schnable, J. C., Schnable, P. S., & Dong, L. (2019). Continuous monitoring of soil nitrate using a miniature sensor with poly(3-octyl-thiophene) and molybdenum disulfide nanocomposite. *ACS Applied Materials & Interfaces*, *11*(32), 29195–29206. https://doi.org/10.1021/acsami.9b07120

Artigas, J., Beltran, A., Jiménez, C., Baldi, A., Mas, R., Domıńguez, C., & Alonso, J. (2001). Application of ion sensitive field effect transistor based sensors to soil analysis. *Computers and Electronics in Agriculture*, *31*(3), 281–293. https://doi.org/10.1016/S0168-1699(00)00187-3

Bland, J. M., & Altman, D. G. (1999). Measuring agreement in method comparison studies. *Statistical Methods in Medical Research*, *8*(2), 135–160. https://doi.org/10.1177/096228029900800204

Breunig, F. M., Galvão, L. S., Dalagnol, R., Santi, A. L., Della Flora, D. P., & Chen, S. (2020). Assessing the effect of spatial resolution on the delineation of management zones for smallholder farming in southern Brazil. *Remote Sensing Applications: Society and Environment*, *19*, 100325. https://doi.org/10.1016/j.rsase.2020.100325

Capó, M., Pérez, A., & Lozano, J. A. (2020). An efficient K-means clustering algorithm for tall data. *Data Mining and Knowledge Discovery*, *34*(3), 776–811. https://doi.org/10.1007/s10618-020-00678-9

Cullmann, A., Sundermann, G., Wägner, N., von, H. C., & Kemfert, C. (2022). DIW weekly report: Water resources in Germany: Increasingly polluted and regionally overused. *Deutsches Institut für Wirtschaftsforschung eV*, *50*(49), 307–315. https://doi.org/10.18723/diw_dwr:2022-49-1

Deumlich, D., Ellerbrock, R. H., & Mo, F. (2018). Estimating carbon stocks in young moraine soils affected by erosion. *Catena*, *162*, 51–60. https://doi.org/10.1016/j.catena.2017.11.016

Donat, M., Geistert, J., Grahmann, K., & Bellingrath-Kimura, S. D. (2023). Field path optimization to reduce headland and turning maneuvers at regional scales: Automated detection of cultivation direction in the state of Brandenburg, Germany. *Precision Agriculture*, *24*(5), 2126–2147. https://doi.org/10.1007/s11119-023-10033-9

Donat, M., Geistert, J., Grahmann, K., Bloch, R., & Bellingrath-Kimura, S. D. (2022). Patch cropping- a new methodological approach to determine new field arrangements that increase the multifunctionality of agricultural landscapes. *Computers and Electronics in Agriculture*, *197*, 106894. https://doi.org/10.1016/j.compag.2022.106894

DWD Climate Data Center. (2023). *Deutscher Wetterdienst (German weather service) climate data center: Daily station observations precipitation height in mm for Germany, version v21.3*. https://cdc.dwd.de/portal/202209231028/mapview

Eckelmann, W., Sponagel, H., Grottenthaler, W., Hartmann, K.-J., Hartwich, R., Janetzko, P., Joisten, H., Kühn, D., Sabel, K.-J., & Traidl, R. (2005). *Bodenkundliche Kartieranleitung. KA5*. https://www.schweizerbart.de/publications/detail/isbn/9783510959204?l=EN

FarmLab—Stenon. (2024). *Soil analysis revolutionized: Optimize inputs & maximize yields*. https://stenon.io/en/

GeoBasis-DE/LGB. (2023). *Digital terrain model*. https://data.geobasis-bb.de/geobasis/daten/dgm/

Georgi, C., Spengler, D., Itzerott, S., & Kleinschmit, B. (2018). Automatic delineation algorithm for site-specific management zones based on satellite remote sensing data. *Precision Agriculture*, *19*(4), 684–707. https://doi.org/10.1007/s11119-017-9549-y

German Agronomic Society. (2021). *Stenon FarmLab—mit Softwareversion d-1.3.0 und Kalibriermodell p-2.1.0*. https://www.dlg.org/de/landwirtschaft/tests/pruefberichte/mess-und-prueftechnik/test-stenon-farmlab

Gracia-Romero, A., Rufo, R., Gómez-Candón, D., Soriano, J. M., Bellvert, J., Yannam, V. R. R., Gulino, D., & Lopes, M. S. (2023). Improving in-season wheat yield prediction using remote sensing and

26396696, 2025, 1, Downloaded from https://acsess.onlinelibrary.wiley.com/doi/10.1002/agg2.70051 by Leibniz Institut Für Agrarlandschaftsforschung (Zalf) e., Wiley Online Library on [25/02/2025]. See the Terms and Conditions (https://onlinelibrary.wiley.com/terms-and-conditions) on Wiley Online Library for rules of use; OA articles are governed by the applicable Creative Commons License

additional agronomic traits as predictors. *Frontiers in Plant Science*, *14*, 1063983. https://doi.org/10.3389/fpls.2023.1063983

Grahmann, K., Reckling, M., Hernández-Ochoa, I., Donat, M., Bellingrath-Kimura, S., & Ewert, F. (2024). Co-designing a landscape experiment to investigate diversified cropping systems. *Agricultural Systems*, *217*, 103950. https://doi.org/10.1016/j.agsy.2024.103950

Grahmann, K., Zwink, M., Barkusky, D., Verch, G., & Sommer, M. (2023). The dilemma of analytical method changes for soil organic carbon in long-term experiments. *European Journal of Soil Science*, *74*(2), e13362. https://doi.org/10.1111/ejss.13362

Guarneri, J., & Weih, R. (2012). Comparing methods for interpolation to improve raster digital elevation models. *Journal of the Arkansas Academy of Science*, *66*(1), 77–81. https://doi.org/10.54119/jaas.2012.6609

Guerrero, A., De Neve, S., & Mouazen, A. M. (2021a). Chapter one—Current sensor technologies for in situ and on-line measurement of soil nitrogen for variable rate fertilization: A review. In D. L. Sparks (Ed.), *Advances in agronomy* (pp. 1–38). Academic Press. https://doi.org/10.1016/bs.agron.2021.02.001

Guerrero, A., De Neve, S., & Mouazen, A. M. (2021b). Data fusion approach for map-based variable-rate nitrogen fertilization in barley and wheat. *Soil and Tillage Research*, *205*, 104789. https://doi.org/10.1016/j.still.2020.104789

Henrich, V., Götze, C., & Krauss, G. (2012). *IDB—Index database*. https://www.indexdatabase.de/

Javadi, S. H., Guerrero, A., & Mouazen, A. M. (2022). Clustering and smoothing pipeline for management zone delineation using proximal and remote sensing. *Sensors*, *22*(2), 645. https://doi.org/10.3390/s22020645

Kernecker, M., Knierim, A., Wurbs, A., Kraus, T., & Borges, F. (2020). Experience versus expectation: Farmers' perceptions of smart farming technologies for cropping systems across Europe. *Precision Agriculture*, *21*(1), 34–50. https://doi.org/10.1007/s11119-019-09651-z

Kharel, T. P., Bhandari, A. B., Mubvumba, P., Tyler, H. L., Fletcher, R. S., & Reddy, K. N. (2023). Mixed-species cover crop biomass estimation using planet imagery. *Sensors*, *23*(3), 1541. https://doi.org/10.3390/s23031541

Kim, H.-J., Hummel, J. W., Sudduth, K. A., & Motavalli, P. P. (2007). Simultaneous analysis of soil macronutrients using ion-selective electrodes. *Soil Science Society of America Journal*, *71*(6), 1867–1877. https://doi.org/10.2136/sssaj2007.0002

Knowles, O., & Dawson, A. (2018). Current soil sampling methods—A review. In L. D. Currie & C. L. Christensen (Eds.), *Farm environmental planning—Science, policy and practice* (Occasional Report No. 31). Fertilizer and Lime Research Centre, Massey University. http://flrc.massey.ac.nz/publications.html

Koch, T., Deumlich, D., Chifflard, P., Panten, K., & Grahmann, K. (2023). Using model simulation to evaluate soil loss potential in diversified agricultural landscapes. *European Journal of Soil Science*, *74*(1), e13332. https://doi.org/10.1111/ejss.13332

Kuester, T., & Spengler, D. (2018). Structural and spectral analysis of cereal canopy reflectance and reflectance anisotropy. *Remote Sensing*, *10*(11), 1767. https://doi.org/10.3390/rs10111767

Li, K., Zhao, Y., Yuan, X., Zhao, H., Wang, Z., Li, S., & Malhi, S. S. (2012). Comparison of factors affecting soil nitrate nitrogen and ammonium nitrogen extraction. *Communications in Soil Science and Plant Analysis*, *43*(3), 571–588. https://doi.org/10.1080/00103624.2012.639108

Li, Y., Yang, Q., Chen, M., Wang, M., & Zhang, M. (2019). An ISE-based on-site soil nitrate nitrogen detection system. *Sensors*, *19*(21), 4669. https://doi.org/10.3390/s19214669

Liu, J., Cai, H., Chen, S., Pi, J., & Zhao, L. (2023). A review on soil nitrogen sensing technologies: Challenges, progress and perspectives. *Agriculture*, *13*(4), 743. https://doi.org/10.3390/agriculture13040743

Mahi, H., Farhi, N., Labed, K., & Benhamed, D. (2018). The silhouette index and the K-harmonic means algorithm for multispectral satellite images clustering. In *2018 International conference on applied smart systems (ICASS)* (pp. 1–6). IEEE. https://doi.org/10.1109/ICASS.2018.8652068

Mahmood, H. S., Hoogmoed, W. B., & van Henten, E. J. (2012). Sensor data fusion to predict multiple soil properties. *Precision Agriculture*, *13*(6), 628–645. https://doi.org/10.1007/s11119-012-9280-7

Maldaner, L. F., Canata, T. F., & Molin, J. P. (2016). *Processing yield data from two or more combines* [Conference presentation]. 13th International Conference on Precision Agriculture, St. Louis, MO.

Metzger, K., & Bragazza, L. (2024). Prediction of nitrogen, active carbon, and organic carbon-to-clay ratio in agricultural soils by in-situ spectroscopy. *European Journal of Soil Science*, *75*(3), e13508. https://doi.org/10.1111/ejss.13508

Mezera, J., Lukas, V., Horniaček, I., Smutný, V., & Elbl, J. (2022). Comparison of proximal and remote sensing for the diagnosis of crop status in site-specific crop management. *Sensors*, *22*(1), 19. https://doi.org/10.3390/s22010019

Najdenko, E., Lorenz, F., Dittert, K., & Olfs, H.-W. (2024). Rapid in-field soil analysis of plant-available nutrients and pH for precision agriculture—A review. *Precision Agriculture*, *25*(6), 3189–3218. https://doi.org/10.1007/s11119-024-10181-6

Nawar, S., Corstanje, R., Halcro, G., Mulla, D., & Mouazen, A. M. (2017). Chapter four—Delineation of soil management zones for variable-rate fertilization: A review. In D. L. Sparks (Ed.), *Advances in agronomy* (pp. 175–245). Academic Press. https://doi.org/10.1016/bs.agron.2017.01.003

Nogueira Martins, R., Magalhães Valente, D. S., Fim Rosas, J. T., Souza Santos, F., Lima Dos Santos, F. F., Nascimento, M., & Campana Nascimento, A. C. (2020). Site-specific nutrient management zones in soybean field using multivariate analysis: An approach based on variable rate fertilization. *Communications in Soil Science and Plant Analysis*, *51*(5), 687–700. https://doi.org/10.1080/00103624.2020.1729793

Oldoni, H., Silva Terra, V. S., Timm, L. C., Júnior, C. R., & Monteiro, A. B. (2019). Delineation of management zones in a peach orchard using multivariate and geostatistical analyses. *Soil and Tillage Research*, *191*, 1–10. https://doi.org/10.1016/j.still.2019.03.008

Reddy, G. P. O. (2018). Remote sensing and GIS in digital terrain modeling. In G. P. O. Reddy & S. K. Singh (Eds.), *Geospatial technologies in land resources mapping, monitoring and management, geotechnologies and the environment* (pp. 201–222). Springer International Publishing. https://doi.org/10.1007/978-3-319-78711-4_11

Smolka, M., Puchberger-Enengl, D., Bipoun, M., Klasa, A., Kiczkajlo, M., Śmiechowski, W., Sowiński, P., Krutzler, C., Keplinger, F., & Vellekoop, M. J. (2017). A mobile lab-on-a-chip device for on-site soil nutrient analysis. *Precision Agriculture*, *18*(2), 152–168. https://doi.org/10.1007/s11119-016-9452-y

Sundermann, G., Wägner, N., Cullmann, A., von Hirschhausen, C. R., & Kemfert, C. (2020). Nitrate pollution of groundwater long exceeding trigger value: Fertilization practices require more transparency

26396696, 2025, 1, Downloaded from https://acsess.onlinelibrary.wiley.com/doi/10.1002/agg2.70051 by Leibniz Institut Für Agrarlandschaftsforschung (Zalf) e., Wiley Online Library on [25/02/2025]. See the Terms and Conditions (https://onlinelibrary.wiley.com/terms-and-conditions) on Wiley Online Library for rules of use; OA articles are governed by the applicable Creative Commons License

and oversight. *DIW Weekly Report*, *10*(8/9), 61–72. https://doi.org/10.18723/diw_dwr:2020-8-1

Tsakiridis, N. L., Tziolas, N., Dimitrakos, A., Galanis, G., Ntonou, E., Tsirika, A., Terzopoulou, E., Kalopesa, E., & Zalidis, G. C. (2017). Predicting soil properties for sustainable agriculture using vis-NIR spectroscopy: A case study in northern Greece. In *Fifth international conference on remote sensing and geoinformation of the environment (RSCy2017)* (pp. 451–458). SPIE. https://doi.org/10.1117/12.2277905

Vallentin, C., Dobers, E. S., Itzerott, S., Kleinschmit, B., & Spengler, D. (2020). Delineation of management zones with spatial data fusion and belief theory. *Precision Agriculture*, *21*(4), 802–830. https://doi.org/10.1007/s11119-019-09696-0

van de Schoot, R., & Miočević, M., Eds. (2020). *Small sample size solutions: A guide for applied researchers and practitioners*. Routledge. https://doi.org/10.4324/9780429273872

Vikuk, V., Spirkaneder, A., Noack, P., & Duemig, A. (2024). Validation of a sensor-system for real-time measurement of mineralized nitrogen in soils. *Smart Agricultural Technology*, *7*, 100390. https://doi.org/10.1016/j.atech.2023.100390

Viscarra Rossel, R. A., & Bouma, J. (2016). Soil sensing: A new paradigm for agriculture. *Agricultural Systems*, *148*, 71–74. https://doi.org/10.1016/j.agsy.2016.07.001

Xue, J., & Su, B. (2017). Significant remote sensing vegetation indices: A review of developments and applications. *Journal of Sensors*, *2017*, e1353691. https://doi.org/10.1155/2017/1353691

Ye, J. Y., Tian, W. H., & Jin, C. W. (2022). Nitrogen in plants: From nutrition to the modulation of abiotic stress adaptation. *Stress Biology*, *2*(1), Article 4. https://doi.org/10.1007/s44154-021-00030-1

Yeshno, E., Arnon, S., & Dahan, O. (2019). Real-time monitoring of nitrate in soils as a key for optimization of agricultural productivity and prevention of groundwater pollution. *Hydrology and Earth System Sciences*, *23*(9), 3997–4010. https://doi.org/10.5194/hess-23-3997-2019

Zhang, J., Guerrero, A., & Mouazen, A. M. (2021). Map-based variable-rate manure application in wheat using a data fusion approach. *Soil and Tillage Research*, *207*, 104846. https://doi.org/10.1016/j.still.2020.104846

Zhang, R., & Wienhold, B. J. (2002). The effect of soil moisture on mineral nitrogen, soil electrical conductivity, and pH. *Nutrient Cycling in Agroecosystems*, *63*(2), 251–254. https://doi.org/10.1023/A:1021115227884

Zhang, S., Huang, J., Wang, Y., Shen, Q., Mu, L., & Liu, Z. (2017). Spatiotemporal heterogeneity of soil available nitrogen during crop growth stages on mollisol slopes of Northeast China. *Land Degradation & Development*, *28*(3), 856–869. https://doi.org/10.1002/ldr.2610

Zhao, J., De Notaris, C., & Olesen, J. E. (2020). Autumn-based vegetation indices for estimating nitrate leaching during autumn and winter in arable cropping systems. *Agriculture, Ecosystems & Environment*, *290*, 106786. https://doi.org/10.1016/j.agee.2019.106786

SUPPORTING INFORMATION

Additional supporting information can be found online in the Supporting Information section at the end of this article.

How to cite this article: Hossain, M. T., Donat, M., Tougma, I. A., Bellingrath-Kimura, S. D., & Grahmann, K. (2025). Nitrogen-based proximal sensing and data fusion for management zone delineation. *Agrosystems, Geosciences & Environment*, *8*, e70051. https://doi.org/10.1002/agg2.70051

26396696, 2025, 1, Downloaded from https://acsess.onlinelibrary.wiley.com/doi/10.1002/agg2.70051 by Leibniz Institut Für Agrarlandschaftsforschung (Zalf) e., Wiley Online Library on [25/02/2025]. See the Terms and Conditions (https://onlinelibrary.wiley.com/terms-and-conditions) on Wiley Online Library for rules of use; OA articles are governed by the applicable Creative Commons License